Sounding the Solar Cycle with Helioseismology: Implications for Asteroseismology

By W. J. Chaplin

1. Introduction

My brief for the IAC Winter School was to cover observational results on helioseismology, flagging where possible implications of those results for the asteroseismic study of solar-type stars. My desire to make such links meant that I concentrated largely upon results for low angular-degree (low-l) solar p modes, in particular results derived from "Sun-as-a-star" observations (which are of course most instructive for the transfer of experience from helioseismology to asteroseismology). The lectures covered many aspects of helioseismology – modern helioseismology is a diverse field. In these notes, rather than discuss each aspect to a moderate level of detail, I have instead made the decision to concentrate upon one theme, that of "sounding" the solar activity cycle with helioseismology. I cover the topics from the lectures and I also include some new material, relating both to the lecture topics and other aspects I did not have time to cover. Implications for asteroseismology are developed and discussed throughout.

The availability of long timeseries data on solar-type stars, courtesy of the NASA *Kepler* Mission (Gilliland et al. 2010; Chaplin et al. 2010) and the French-led CoRoT satellite (Appourchaux et al. 2008), is now making it possible to "sound" stellar cycles with asteroseismology. The prospects for such studies have been considered in some depth (e.g., Chaplin et al. 2007, 2008a; Metcalfe et al. 2008; Karoff et al. 2009), and in the last year the first convincing results on stellar-cycle variations of the p-mode frequencies of a solar-type star (the F-type star HD49933) were reported by García et al. (2010). This result is important for two reasons: first, the obvious one of being the first such result, thereby demonstrating the feasibility of such studies; and second, the period of the stellar cycle was evidently significantly shorter than the 11-yr period of the Sun (probably between 1 and 2 yr). If other similar stars show similar short-length cycles, there is the prospect of being able to "sound" perhaps two or more complete cycles of such stars with *Kepler* (assuming the mission is extended, as expected, to 6.5 yr or more). The results on HD49933 may be consistent with the paradigm that stars divide into two groups, activity-wise, with stars in each group displaying a similar number of rotation periods per cycle period (e.g., see Böhm-Vitense 2007), meaning solar-type stars with short rotation periods – HD49933 has a surface rotation period of about 3 days – tend to have short cycle periods. We note that Metcalfe et al. (2010) recently found another F-type star with a short (1.6 yr) cycle period (using chromospheric H & K data). Extension of the *Kepler* Mission will of course also open the possibility of detecting full swings in activity in stars with cycles having periods up to approximately the length of the solar cycle.

The rest of my notes break down as follows. Section 2 gives an introductory overview of the solar cycle, as seen in helioseismic data. A brief history of observations of solar cycle changes in low-angular degree (low-l) solar p modes is given in Section 2.1. Then, in Section 2.2, we consider the causes of the observed changes in the mode frequencies; and in Section 2.3, we discuss variations in the mode powers and damping rates, and what the relative sizes of those changes imply for the underlying cause.

Section 3 considers several subtle ways in which the stellar activity cycles can affect values of, and inferences made from, the mode parameters. Concepts are introduced using the example of the solar cycle, and the impact it has on low-l p modes observed in Sun-as-a-star data. Implications for asteroseismic observations of solar-type stars are then developed. We start in Section 3.1 with a discussion of the impact of stellar activity on estimates of the mode frequencies. This is followed in Section 3.2 by a similar discussion for frequency separation ratios. Finally, Section 3.3 explains how mode peaks in the frequency-power spectrum can be "distorted" by stellar cycles, rendering commonly used fitting models inappropriate.

In Section 4 we develop a simple model to illustrate the impact on the mode frequencies of the range in latitudes covered by near-surface magnetic activity on solar-type stars, and discuss how the angle of inclination can affect significantly the observed frequency shifts (because that angle affects which mode components are visible in the observations). We also show how measurements of the frequency shifts of modes having different angular and azimuthal degrees may be used to make inference on the spatial distribution of the near-surface magnetic activity on solar-type stars.

We end in Section 5 by thinking somewhat longer-term, and consider how much low-l data would be needed to measure *evolutionary* changes of the solar p-mode frequencies.

2. The seismic solar cycle: overview

A rich, and diverse, body of observational data is now available on temporal variations of the properties of the global solar p modes. The signatures of these variations are correlated strongly with the well-known 11-year cycle of surface activity. The search for temporal variations of the p-mode properties began in the early 1980s, following accumulation of several years of global seismic data. The first positive result was reported by Woodard & Noyes (1985), who found evidence in observations made by the Active Cavity Radiometer Irradiance Monitor (ACRIM) instrument, on board the Solar Maximum Mission (SMM) satellite, for a systematic decrease of the frequencies of low-l p modes between 1980 and 1984. The first year coincided with high levels of global surface activity, while during the latter period activity levels were much lower. The modes appeared to be responding to the Sun's 11-year cycle of magnetic activity. Woodard & Noyes found that the frequencies of the most prominent modes had decreased by roughly 1 part in 10 000 between the activity maximum and minimum of the cycle. By the late 1980s, an in-depth study of frequency variations of global p modes, observed in the Big Bear data, had demonstrated that the agent of change was confined to the outer layers of the interior (Libbrecht & Woodard, 1990).

Accumulation of data from the new networks and instruments has made it possible to study the frequency variations to unprecedented levels of detail, and has revealed signatures of subtle, structural change in the sub-surface layers. The discovery of solar-cycle variations in mode parameters associated with the excitation and damping (e.g., power, damping rate, and peak asymmetry) followed. Patterns of flow that penetrate a substantial fraction of the convection zone have also been uncovered as well as possibly signatures of changes in the rotation rate of the layers that straddle the tachocline, and much more recently evidence for a quasi-periodic 2-yr signal, superimposed on the solar-cycle variations of the mode frequencies.

The modern seismic data give unprecedented precision on measurements of frequency shifts. Examples of average frequency shifts for low-l data are shown in Fig. 1, for Sun-as-a-star data collected by the ground-based Birmingham Solar-Oscillations Network (BiSON), and Global Oscillations at Low Frequency (GOLF) instrument on board
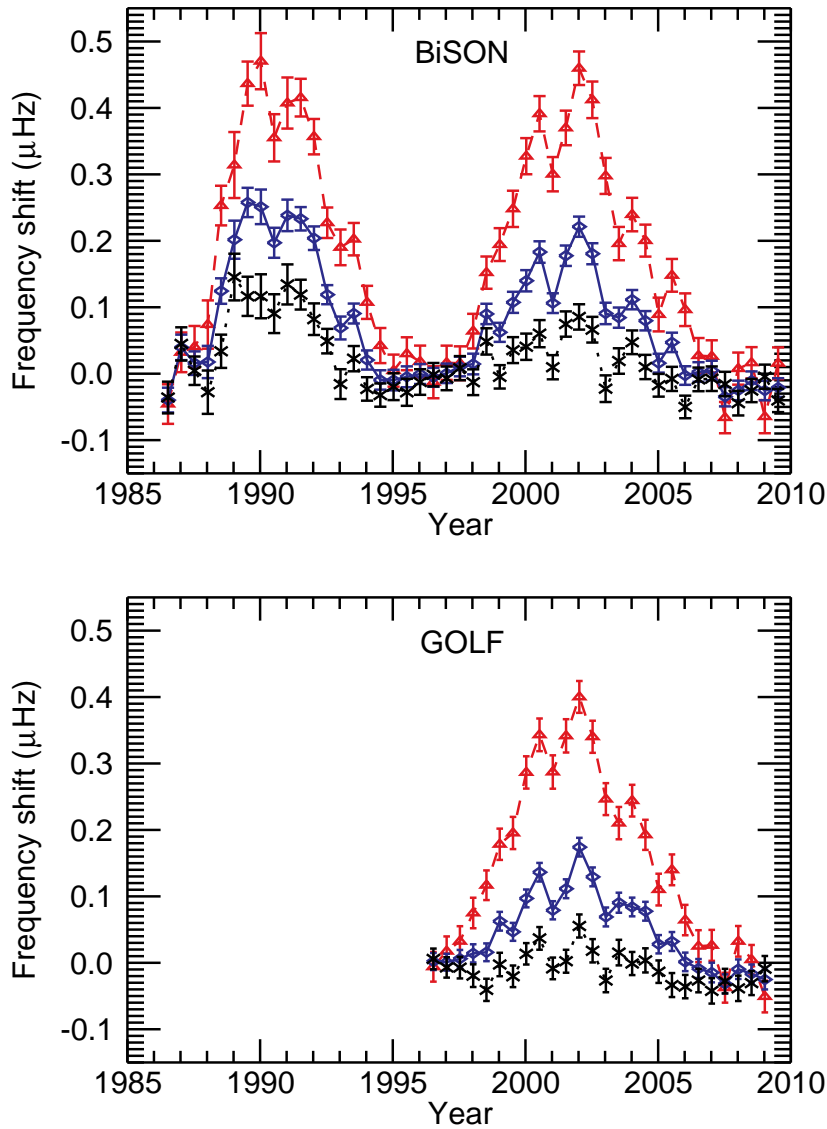
FIGURE 1. Average frequency shifts of most prominent low-l solar p modes, as measured in BiSON data (top panel) and GOLF data (bottom panel) over the last two 11-yr activity cycles. The three curves show results for averages made over different ranges in frequency: 1880 to 3710 μHz (diamonds, joined by solid line); 1880 to 2770 μHz (crosses, joined by dotted line); 2820 to 3710 μHz (triangles, joined by dashed line). (From Fletcher et al. 2010.)

the ESA/NASA Solar and Heliospheric Observatory (SOHO). From observations of the medium-l frequency shifts it is possible to produce surface maps showing the strength of the solar-cycle shifts as a function of latitude and time (Howe, Komm, & Hill, 2002), like the example shown in Figure 2 (which is made from Global Oscillations Network Group (GONG) data). These maps bear a striking resemblance to the butterfly diagrams that show spatial variations in the strength of the surface magnetic field over time. The implication is that the frequency shift of a given mode depends on the strength of that component of the surface magnetic field that has the same spherical harmonic projection on the surface. Similar maps may also be made for variations observed in the p-mode
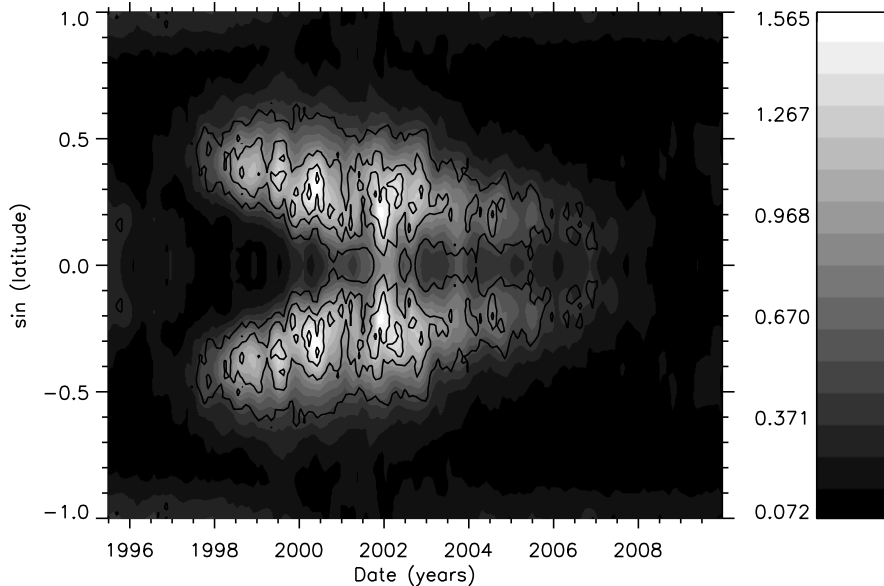
FIGURE 2. Mode frequency shifts (in μHz) as a function of time and latitude. The values come from analysis of GONG data. The contour lines indicate the surface magnetic activity. (Figure courtesy of R. Howe.)

powers and damping rates (Komm, Howe, & Hill, 2002), which, like the frequency maps, show a close spatial and temporal correspondence with the evolution of active-region field (Figure 3).

2.1. *The seismic solar cycle at low angular degree*

As noted above, the first evidence for activity-related changes to the low-l p modes of the Sun was reported by Woodard & Noyes (1985). These changes were soon confirmed (and the results extended) by Pallé et al. (1989) and Elsworth et al. (1990). Almost two decades on, there now exists an extensive literature devoted to studies of low-l mode parameter variations. Since the frequencies are by far the most precisely determined parameters, it is hardly surprising that analyses of the frequencies threw up the first positive results for solar-cycle changes. Evidence for changes in mode power followed next (Pallé et al. 1990a; Anguera-Gubau et al. 1992; Elsworth et al. 1994). The first tentative claims for changes in mode linewidth (damping) were made by Pallé et al. (1990b). Subsequently, Toutain & Wehrli (1997) and Appourchaux (1998) provided stronger evidence in support of an increase in damping with activity, and these claims were confirmed beyond all doubt by Chaplin et al. (2000). (Komm, Howe & Hill (2000) did likewise for medium l modes at about the same time.) Peak asymmetry is the most recent addition to the list of parameters that show solar-cycle variations (Jiménez-Reyes et al. 2007). Careful measurement of variations in the powers, damping rates and peak asymmetries – all parameters associated with the excitation and damping – are allowing studies to be made of the impact of the solar cycle on the convection properties in the near-surface layers.

Frequencies of modes below $\approx 4000 \, \mu$Hz are observed to increase with increasing ac-
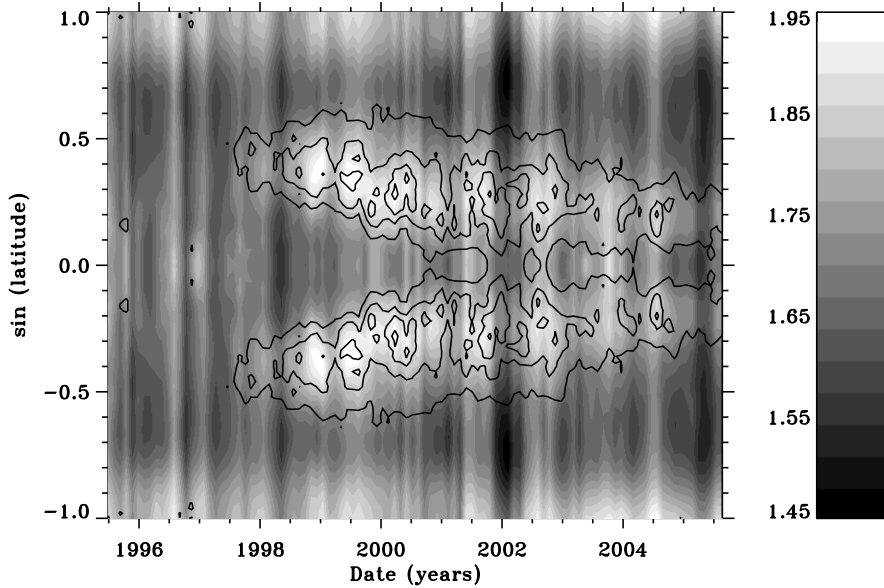
FIGURE 3. Mode linewidth (in μHz) as a function of time and latitude. The values come from analysis of GONG data. The contour lines indicate the surface magnetic activity. (Courtesy of R. Howe.)

tivity. For the most prominent modes at around $3000\,\mu$Hz, the size of the shift is about $0.4\,\mu$Hz between activity minimum and maximum. Furthermore, higher frequency modes experience a larger shift than their lower-frequency counterparts. This frequency dependence suggests that the perturbations responsible for the frequency shifts are located very close to the solar surface. The upper turning points of the modes – which for low-degree modes are effectively independent of l – lie deeper in the Sun for low-frequency modes than they do for high-frequency modes: higher-frequency modes are as such more sensitive to surface perturbations.

That the shifts do not scale like ν_{nl}/L, where ν_{nl} is mode frequency and $L = \sqrt{l(l+1)}$, rules out the possibility that the perturbation is spread throughout a significant fraction of the solar interior. This may be understood by thinking classically, in terms of ray paths followed by the acoustic waves. When a wave reaches the lower turning point of its cavity it will by definition be moving horizontally, and its phase speed will be equal to

$$c = \frac{\omega_{nl}}{k} = \frac{2\pi\nu_{nl}R}{\sqrt{l(l+1)}} \propto \nu_{nl}/L, \qquad (2.1)$$

where k is the horizontal wavenumber and R the outer cavity radius. The ratio ν_{nl}/L therefore maps to the location of the lower boundary of the cavity, and hence the cavity size. Since the shifts do not scale like this ratio, we conclude that the perturbation must be confined within a narrow layer, and not spread so widely that it covers the entirety of the cavities of many of the modes.

At frequencies above $4000\,\mu$Hz the size of the shift decreases, and also changes sign above $\simeq 4500\,\mu$Hz meaning that these very high-frequency modes suffer a reduction in

frequency as activity levels rise (Anguera-Gubau et al. 1992; Chaplin et al. 1998; Jiménez-Reyes et al. 2001; Gelly et al. 2002; Salabert et al. 2004).

Detailed comparison of the low-l frequency shifts with changes in various disc-averaged proxies of global surface activity provides further tangible input to the solar cycle studies. This is because different proxies show differing sensitivity to various components of the surface activity. While the changes in frequency are observed to correlate fairly well with contemporaneous changes in global proxies, the match is far from perfect. Jiménez-Reyes et al. (1998) were the first to show that the relation of the frequency shifts to variations in the proxies was markedly different on the rising and falling parts of the 11-yr Schwabe cycle. Since the magnitudes of the shifts should reflect the different spatial sensitivities of modes of different angular and azimuthal degree to the time-dependent variation of the surface distribution of the activity, a better choice for the activity proxy would clearly be one that has been decomposed to have a similar spatial distribution as the mode under study. Chaplin et al. (2004a) and Jiménez-Reyes et al. (2004) have shown that the sizes of the low-l shifts do indeed scale better with activity proxies that have the same spherical harmonic projection as the modes.

Chaplin et al., (2007b) compared frequency changes in 30 years of BiSON data with variations in six well-known activity proxies. Interestingly, they found that only activity proxies having good sensitivity to the effects of weak-component magnetic flux – which is more widely distributed in latitude than the strong flux in the active regions – were able to follow the frequency shifts consistently over the three cycles.

The unusual behaviour during the most recent solar minimum (straddling solar cycles 23 and 24) of many diagnostics and probes of solar activity has raised considerable interest and debate in the scientific community (e.g., see the summary by Sheeley 2010). The minimum was unusually, and unexpectedly, extended and deep. Polar magnetic fields were very weak, and the open flux was diminished compared to other preceding minima.

Helioseismology has been used to probe the behaviour of sub-surface flows during the minimum. Howe et al. (2009) found that the equatorward progression of the lower branches of the so-called torsional oscillations (east-west flows) was late in starting compared to previous cycles. They flagged this delayed migration as a possible pre-cursor of the delayed onset of cycle 24. The meridional (north-south) flow also carries a signature of the solar cycle, which converges toward the active-region latitudes and also intensifies in strength as activity increases: González-Hernández (2010) found that during the current minimum this component had developed to detectable levels even before the visual onset of magnetic activity on the solar surface.

The globally coherent acoustic properties of the recent solar minimum have been studied extensively with low-degree p modes (by Broomhall et al. 2009 and Salabert et al. 2009) and medium-degree p modes (Tripathy et al. 2010). These studies have shown that while the surface proxies of activity (e.g., the 10.7-cm radio flux) were quiescent and very stable during the minimum, the p-mode frequencies showed much more variability. Tripathy et al. (2010) noted further surprising behaviour compared to the previous cycle 22-23 minimum, i.e., an apparent anti-correlation of the p-mode frequency shifts and the surface proxies of activity.

Broomhall et al. (2009) had suggested the possible presence of a quasi-biennial modulation of the frequencies of the low-degree modes, superimposed upon the well-established ~ 11-yr variation of the frequencies. This has since been confirmed by further in-depth analysis, which reveals a signature that is consistent in the frequencies extracted from BiSON and GOLF data (Fletcher et al. 2010), as shown in Fig. 4. This plots the frequency residuals that remain after the long-term solar-cycle variation has been removed from the average frequency shifts. The residuals show significant variability, with a period of
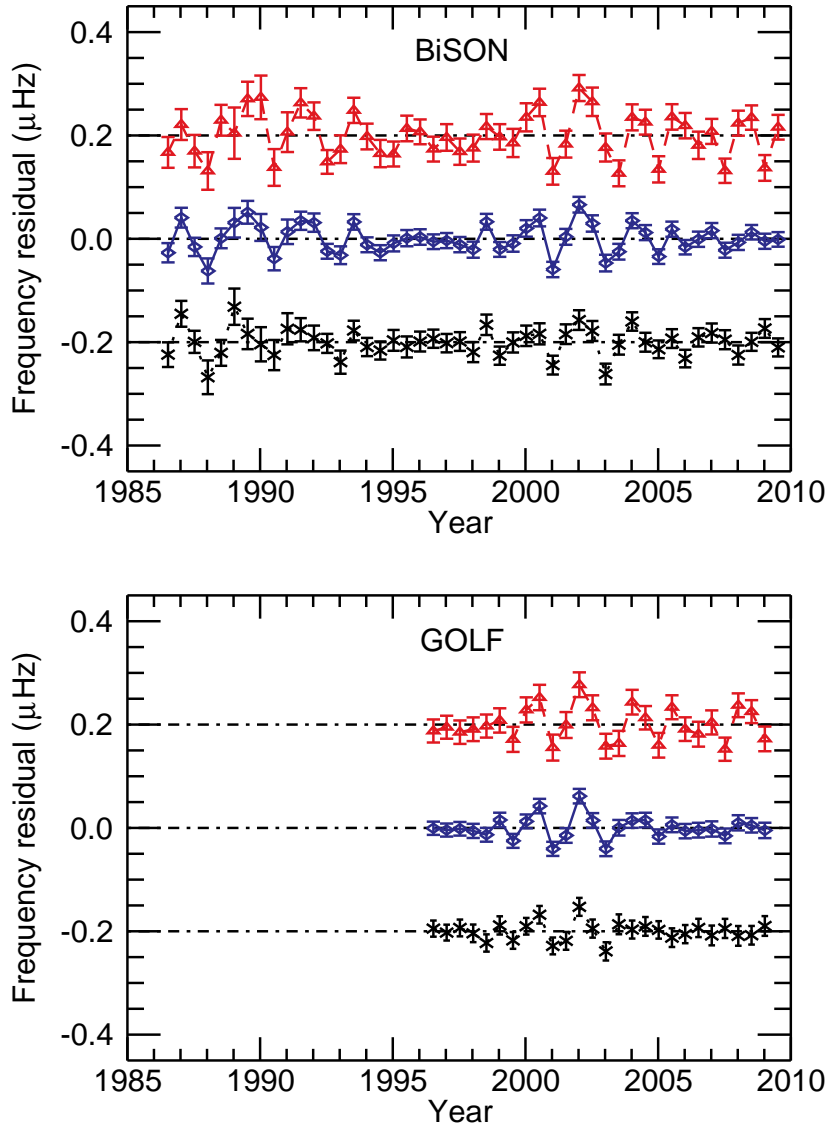
FIGURE 4. Frequency residuals that remain after the long-term solar-cycle variation has been removed from the average frequency shifts of BiSON data (top panel) and GOLF data (bottom panel). The three curves in each panel show results for averages made over different ranges in frequency: 1880 to 3710 μHz (diamonds, joined by solid line); 1880 to 2770 μHz (crosses, joined by dotted line); 2820 to 3710 μHz (triangles, joined by dashed line). (Plot from Fletcher et al. 2009.)

around 2 yr, that variability being more pronounced at times of higher surface activity. The fact that this biennial signature has similar amplitude in the low-frequency *and* the high-frequency modes used in this analysis suggests that its origins lie deeper than the very superficial layers responsible for the 11-year shifts.

Finally in this section on the frequencies, we note that from appropriate combinations of low-l frequencies Verner et al. (2006) uncovered apparent solar-cycle variations in the amplitude of the depression in the adiabatic index, Γ_1, in the He II zone. These variations presumably reflect the impact of the changing activity on the equation of state of the

gas in the layer, and confirmed the findings of Basu and Mandel (2004), who used the more numerous data available from medium-l frequencies.

2.2. *What is the cause of the frequency shifts?*

Broadly speaking, the magnetic fields can affect the modes in two ways. They can do so directly, by the action of the Lorentz force on the gas. This provides an additional restoring force, the result being an increase of frequency, and the appearance of new modes. Magnetic fields can also influence matters indirectly, by affecting the physical properties in the mode cavities and, as a result, the propagation of the acoustic waves within them. This indirect effect can act both ways, to either increase or decrease the frequencies.

We begin this section with a back-of-the-envelope calculation, which makes (an admittedly) approximate prediction of the impact on the frequency of a typical low-l mode of changes in stratification brought about by the near-surface magnetic field in sunspots. The calculation is instructive, in that the size of the predicted frequency shift it gives is broadly in line with the observations, providing further evidence in support of the shifts being caused by near-surface perturbations due to the presence of magnetic field.

As we have seen, frequencies of the most prominent modes increase with increasing magnetic activity. Here, we consider the indirect effect of the near-surface magnetic field on the near-surface properties, and hence the frequencies of these modes. If magnetic fields modify the surface properties in such a way as to reduce the effective size of the mode cavity, the required increase of frequency will result.

In regions of strong magnetic field – such as those occupied by sunspots – there will be a gas pressure deficit (assuming those regions to be in pressure equilibrium with their field-free surroundings). This is because gas and magnetic pressure combine within the magnetic regions, while only gas pressure acts in the field-free regions. Sunspots are also characterized by a reduced temperature, relative to the surroundings. The central part of the spot therefore exhibits a lower pressure, temperature and density than the surroundings, resulting in the so-called Wilson Depression. Values of pressure, temperature and density found at the surface in the field-free plasma are only reached at some depth beneath the surface in strong-field regions. Recent measurements suggest that for a sunspot the typical size of this depression is about 1000 km (Watson et al. 2009).

Let us assume that 1000 km corresponds approximately to the amount, δR, by which the mode cavities are reduced in size beneath sunspots. The fractional area of the solar surface occupied by sunspots reaches $\sim 0.5\%$ at modern cycle maxima. We therefore obtain a net, surface-averaged estimate of δR via

$$\langle \delta R \rangle \approx 0.5\% \times 1000\,\mathrm{km} \approx 5\,\mathrm{km}.$$

The sound speed, c, at the solar surface is approximately $10\,\mathrm{km\,s^{-1}}$, implying a reduction in the travel time in the mode cavity, due to the "shrinkage" at the surface, of

$$\delta T \approx 5\,\mathrm{km}/10\,\mathrm{km\,s^{-1}} \approx 0.5\,\mathrm{s}.$$

The travel time across the cavity, T, is related to the large frequency separation, $\Delta\nu$, via:

$$\Delta\nu \simeq \left(2 \int_0^R \frac{dr}{c} \right)^{-1} \simeq (2T)^{-1}. \tag{2.2}$$

For the Sun, $\Delta\nu = 135\,\mu\mathrm{Hz}$, implying $T \approx 3700\,\mathrm{s}$. The fractional change (reduction) in T is therefore:

$$\delta T/T \simeq 0.5/3700 \simeq 1.4 \times 10^{-4}.$$

Since $\delta\nu/\nu = -\delta T/T$, the predicted increase in frequency of a mode at $\approx 3000\,\mu$Hz will be

$$\delta\nu = 3000 \times 1.4 \times 10^{-4} \simeq 0.4\,\mu\text{Hz}.$$

This estimate is of a very similar size to the observed frequency shifts.

What does detailed modelling suggest? Perhaps the most significant contribution of recent years in this area is that of Dziembowski and Goode (2005). Their results suggest that the indirect effects dominate the perturbations, and that the magnetic fields are too weak in the near-surface layers for the direct effect to contribute significantly to the observed frequency shifts. However, Dziembowski and Goode also found some evidence to suggest that the direct effect may play a more important rôle for low-frequency modes, at depths beneath the surface where the magnetic field is strong enough to give a significant direct contribution to the frequency shifts. We now go on to explain how dependence of the frequency shifts on mode inertia and mode frequency can tell us something about the location and nature of the perturbations.

We begin by noting that when the frequency shifts are multiplied by the mode inertia, and then normalized by the inertia of a radial mode of the same frequency, the modified shifts are found to be a function of frequency alone. This in effect removes any l dependence of the shifts (at fixed frequency, the higher the l, the larger is the observed frequency shift). The observed l dependence may be understood in terms of, for example, a physical interpretation of the mode inertia. The normalized inertia, I_{nl}, may be defined according to (Christensen-Dalsgaard & Berthomieu 1991):

$$I_{nl} = \text{M}_\odot^{-1} \int_V |\xi|^2 \rho dV = 4\pi \text{M}_\odot^{-1} \int_0^R |\xi|^2 \rho r^2 dr = M_{nl}/\text{M}_\odot \qquad (2.3)$$

where ξ is the (surface-normalized) displacement associated with the mode, and the integration is performed over the volume V of the Sun, which has mass $\text{M}_\odot$. The mode mass M_{nl} is therefore the interior mass affected by the perturbations associated with the mode. As l increases, so M_{nl} decreases, and the more sensitive a mode will be to a near-surface perturbation of a given size (giving a larger frequency shift). One may therefore render the shifts l independent by multiplying them by the inertia ratio Q_{nl} (Christensen-Dalsgaard & Berthomieu 1991), which is given by:

$$Q_{nl} = I_{nl}/\bar{I}(\nu_{nl}) \qquad (2.4)$$

Multiplication of the raw shifts by Q_{nl} is indeed seen to collapse the shifts of different l onto a single curve. As shown in Fig. 5, this then allows one to combine data spanning a range in l, which reduces errors, giving tighter constraints on frequency dependence of the shifts.

Chaplin et al. (2001) studied in detail the frequency dependence of the inertia-ratio-corrected shifts, $\delta\nu_{nl}Q_{nl}$, of both low-l modes and medium-l modes up to $l = 150$. They fitted these data to a power law of the form

$$\delta\nu_{nl}Q_{nl} = \frac{c}{I_{nl}}\nu_{nl}^\alpha, \qquad (2.5)$$

where the power-law index is α and c is a constant. They found that $\alpha \simeq 2$ for $\nu \geq 2500\,\mu$Hz, while α is approximately zero for $\nu < 2500\,\mu$Hz. Rabello-Soares et al. (2008) repeated the exercise for medium-l and high-l modes. They extracted very similar behaviour, and, because they had more medium- and high-l data at low frequencies, they were able to extend the analysis to $\nu < 2000\,\mu$Hz where they found that α appears to change sign and go negative. The high-l modes provide important information since they
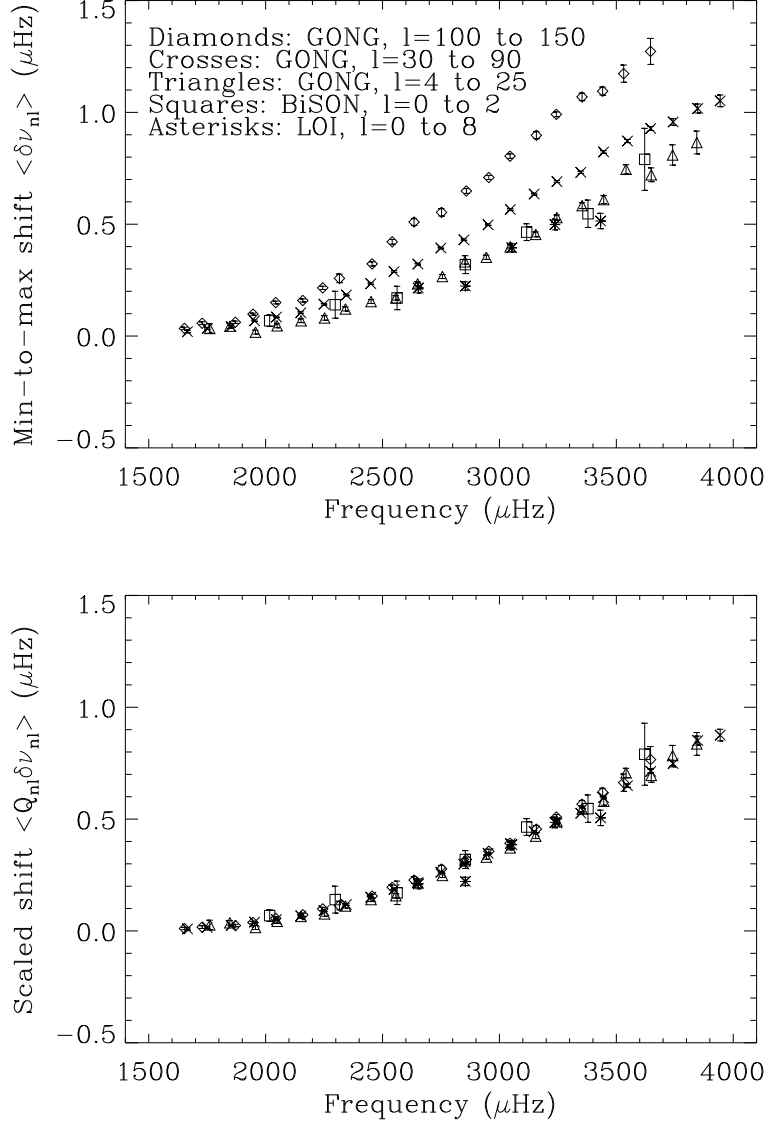
FIGURE 5. Top panel: Frequency shifts, $\delta\nu$, plotted as a function of mode frequency, for results from different instruments over different ranges in l (see plot annotation). Bottom panel: Scaled frequency shifts, after multiplication by the inertia ratio Q_{nl}. (From Chaplin et al. 2001.)

are confined in the layers close to the surface where the physical changes responsible for the frequency shifts are also located.

What do the values of α imply? If the perturbation is located within the photosphere (but is confined to extend over an extent no longer than one pressure scale height), then we might expect $\alpha \simeq 3$ (e.g., Libbrecht & Woodard 1990). If instead the perturbation extends beneath the surface, the frequency dependence will be weaker and α will get smaller (Gough 1990). The observed values of α in the above mentioned frequency regimes are both less than 3, suggesting that the perturbations cannot arise solely in

the photosphere. Since α is smaller for the lower-frequency modes, this suggests that the perturbation extends to greater depths the lower in frequency one goes. This is consistent with the inferences made by Goode & Dziembowski (2005).

2.3. *Solar-cycle variations of mode power and mode damping*

Variations in mode damping have now been uncovered in all the major low-*l* datasets (see Chaplin 2004 and references therein). The trend found is an increase of about 20 per cent between activity minimum and maximum, with some suggestion of the variations being peaked in size at about $\simeq 3000\,\mu$Hz. Mode powers are at the same time observed to decrease by about the same fractional amount, while the mode heights decrease by twice the amount. Use of the analogy of a damped, randomly forced oscillator is particularly instructive for understanding these results.

We define our oscillator according to the equation:

$$\ddot{x}(t) + 2\eta\dot{x}(t) + (2\pi\nu_0)^2 x(t) = K\delta(t - t_0), \tag{2.6}$$

where $x(t)$ is the displacement, ν_0 the natural frequency of the oscillator, η the linear damping constant, and K is the amplitude of the forcing function (assumed to be a random Gaussian variable), with "kicks" applied at times t_0, $\delta(t - t_0)$ being the delta function.

Provided that $\mathcal{F}(\nu)$ – the frequency spectrum of the forcing function – is a slowly-varying function of ν, and $\eta << 2\pi\nu_0$, the power spectral density (PSD) in the frequency domain will be a Lorentzian profile, i.e.,

$$\text{PSD}(\nu) \propto \mathcal{F}(\nu)\left(1 + \left(\frac{\nu - \nu_0}{\eta/2\pi}\right)^2\right)^{-1}. \tag{2.7}$$

This holds for both the spectrum of the displacement, $x(t)$, and the velocity, $\dot{x}(t)$. The FWHM of the peak in cyclic frequency is

$$\Delta = \frac{\eta}{\pi}. \tag{2.8}$$

The maximum power spectral density, or height, of the resonant peak is:

$$H \propto \frac{\mathcal{F}(\nu)}{\eta^2}. \tag{2.9}$$

The total mean-square power (variance in the time domain) is proportional to peak height times width, i.e., $P \propto H\Delta$, so that

$$P \propto \frac{\mathcal{F}(\nu)}{\eta}. \tag{2.10}$$

The energy (kinetic plus potential) of a resonant mode with associated inertia I is given by:

$$E = MP. \tag{2.11}$$

The rate at which energy is supplied to (and dissipated by) the modes, dE/dt, is readily derived by again having recourse to the oscillator analogy. The amplitude of the oscillator is attenuated in time by the factor $\exp(-\eta t)$, and its energy is proportional to the amplitude squared. Hence, we may write

$$E = (\text{constant}) \times \exp(-2\eta t).$$

It follows that:

$$\log E = -2\eta t + \log(\text{constant}),$$

and taking derivatives:

$$dE/dt = -2\eta E. \tag{2.12}$$

If we combine Equations 2.10, 2.11 and 2.12, we have:

$$dE/dt = \dot{E} \propto -\mathcal{F}(\nu)I. \tag{2.13}$$

We may attempt to measure solar-cycle variations in Δ, H, P, E and $\dot{E}$. The parameters that are usually extracted directly by the observers are the widths (Δ) and heights (H) of the peaks in the frequency power spectrum. The mode powers, P, are then estimated from

$$P = \frac{\pi}{2}\Delta H \tag{2.14}$$

(i.e., area under Lorentzian). The E may be computed from the P using model computed inertias, I. We note that fractional changes in E will be the same as those in P (assuming the I do not show any significant changes). Finally, $\dot{E}$ follows from

$$\dot{E} = -\pi E\Delta = -\pi IP\Delta. \tag{2.15}$$

If solar-cycle variations are uncovered in the above parameters, what do they imply for the underlying cause (or causes)? If we think in terms of the basic oscillator parameters – the damping rate η and the forcing function $\mathcal{F}(\nu)$ – Equations 2.8, 2.9, 2.10, 2.11 and 2.13 then imply the following:

$$\delta\Delta\nu/\Delta\nu = \delta\eta/\eta, \tag{2.16}$$

$$\delta H/H = \delta\mathcal{F}(\nu)/\mathcal{F}(\nu) - 2\delta\eta/\eta, \tag{2.17}$$

$$\delta P/P = \delta E/E = \delta\mathcal{F}(\nu)/\mathcal{F}(\nu) - \delta\eta/\eta, \tag{2.18}$$

and

$$\delta\dot{E}/\dot{E} = \delta\mathcal{F}(\nu)/\mathcal{F}(\nu). \tag{2.19}$$

Observations of p modes at low l are consistent with $\delta\dot{E}/\dot{E} = 0$, which in turn implies that $\delta\mathcal{F}(\nu)/\mathcal{F}(\nu) = 0$: the acoustic forcing of the low-l modes remains, on average, constant over the cycle. Any changes that are observed in the other parameters must therefore arise from $\delta\eta/\eta$ alone, and we have that:

$$\delta\Delta\nu/\Delta\nu = -\delta P/P = -\delta H/2H, \tag{2.20}$$

The observed changes in Δ, P and H follow these ratios. We may therefore infer that changes to these parameters are in all likelihood the result of changes to the damping of the low-l modes. Houdek et al. (2001) noted that the high Rayleigh number of the magnetic field could modify the preferred horizontal length-scale of the convection, which in turn could modify the damping rates. Their numerical calculations of the implied changes for low-l modes show reasonable agreement with the observations.

3. Subtle signatures of stellar activity and stellar-cycle variations

Asteroseismic observations of stars will, for the foreseeable future, be limited to obtaining data on low-l modes because of the cancellation effects resulting from unresolved observations of stellar discs. Moreover, the angle of inclination, i, offered by a star also determines which of the low-l components will have non-negligible visibility in the data. The visibility of the radial ($l = 0$) modes is not affected by i, but for the non-radial modes the visibility, $\mathcal{E}(i)_{lm}$ (in power) of a given (l, m) component is assumed to go like

(e.g., Gizon & Solanki 2003):

$$\mathcal{E}(i)_{lm} \propto \frac{(l-|m|)!}{(l+|m|)!} \left(P_l^{|m|}(\cos i) \right)^2 , \tag{3.1}$$

where $P_l^{|m|}$ are Legendre polynomials. The fact that some components may in effect be missing from the data has important implications for the analysis. There are some obvious implications, e.g., it will not be possible to measure frequency splittings of non-radial modes if i is close to 90 degrees – so that the star is viewed rotation-pole on – since only the zonal components ($m = 0$) will have non-negligible visibility. In this section we highlight a more subtle aspect, which relates to the fact that estimates of the frequencies of non-radial modes are affected by the interplay between the effects of near-surface magnetic activity and the relative visibility (or absence) of the mode components. This has consequences for inferences made on solar-type stars. We first introduce and explain the problems using "Sun-as-a-star" helioseismic observations as a test case, before considering the wider implications for asteroseismology. We return later, in Section 4 to discuss the implications for estimation of average frequency shifts of solar-type stars.

3.1. *Explanation and description of frequency bias*

Extant Sun-as-a-star observations are made from a perspective in which the plane of the rotation axis of the Sun is nearly perpendicular to the line-of-sight direction (i.e., i is always close to 90 degrees). This means that only components with $l+m$ even have non-negligible visibility. As we shall explain below, the impact of surface magnetic activity on the arrangement of the components in frequency means it may not then be possible to estimate the true frequency centroid of the multiplet. The frequency centroids carry information on the spherically symmetric component of the internal structure, and are the input data that are required, for example, for hydrostatic structure inversions.

In the complete absence of the near-surface activity, the $l+m$ odd components which are "missing" from the Sun-a-as-a-star data would be an irrelevance. All mode components would be arranged symmetrically in frequency, meaning centroids could be estimated accurately from the subset of visible components. A near-symmetric arrangement is found at the epochs of modern solar-cycle minima (Chaplin et al. 2004b). However, when the observations span a period having medium to high levels of activity – as a long dataset by necessity must – the arrangement of components will no longer be symmetric. The frequencies given by fitting the Sun-as-a-star data will then differ from the true centroids by an amount that is sensitive to l. The l dependence arises because in the Sun-as-a-star data modes of different l comprise visible components having different combinations of l and m; and these different combinations show different responses (in amplitude and phase) to the spatially non-homogeneous surface activity (i.e., as observed in the active bands of latitude for solar-type stars).

These effects are illustrated in Figs. 6 and 7. Fig. 6 is a schematic plot of the arrangement in frequency of the components of an $l = 2$ mode, under circumstances where activity levels are assumed to be negligible. The top panel shows the arrangement in frequency of the various m (as labelled on the ordinate), assuming a rotational frequency splitting of $0.4\,\mu$Hz between adjacent m. The dotted line marks the frequency centroid. The middle panel shows schematically both the placement in frequency (abscissa) and relative visibility in the frequency power spectrum (height on ordinate) of the three mode components that would have non-negligible visibility in the Sun-as-a-star data. The bottom panel shows the Lorentzian peak profiles expected of a mode at the centre of the p-mode spectrum (where peak linewidths are around $1\,\mu$Hz).

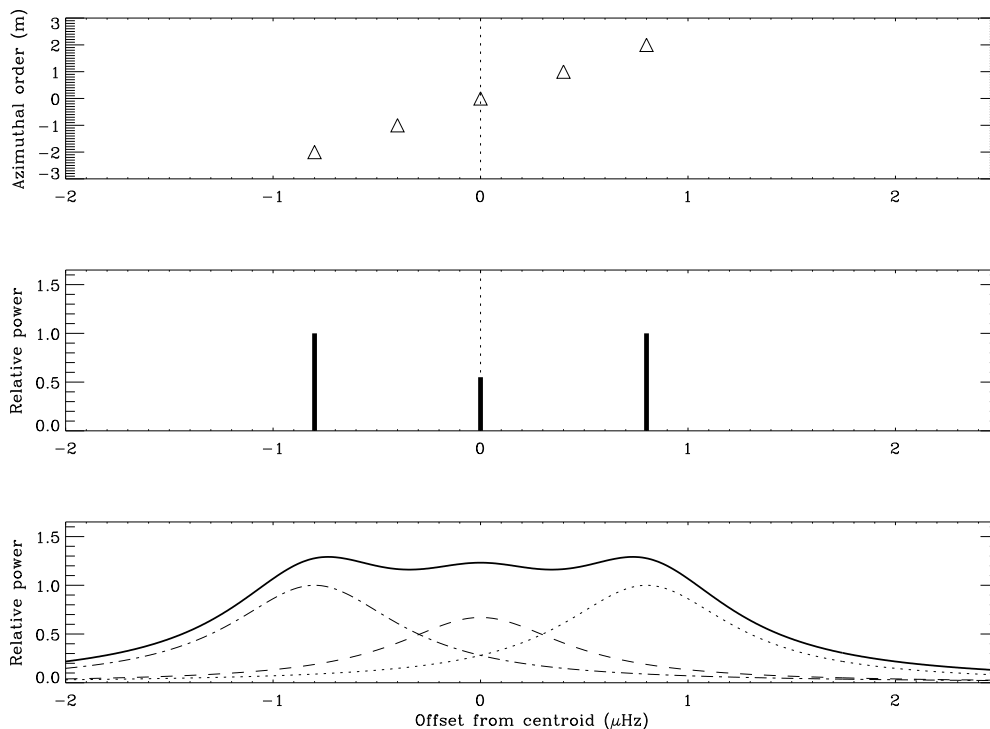Fig. 7 shows the situation at an epoch coinciding with high levels of solar activity.

FIGURE 6. Top panel: Placement in frequency, relative to the frequency centroid of all $2l + 1$ components (abscissa), of the various m (labelled on ordinate) of an $l = 2$ mode during an epoch of negligible solar surface activity. The solid vertical line marks the location of the centroid. Middle panel: placement in frequency (abscissa) and relative visibility in the frequency power spectrum (height on ordinate) of the three mode components that would have non-negligible visibility in the Sun-as-a-star data. Bottom panel: Lorentzian peak profiles expected of an $l = 2$ mode at the centre of the p-mode spectrum (where peak linewidths are around $1\,\mu$Hz).

This activity is most prominent in the active latitudes. The $|m| = 2$ components are more sensitive to acoustic perturbations due to activity that arise in these latitudes than is the $m = 0$ component (as a result of the spatial distribution of the relevant spherical harmonic components). The result is a distortion of the symmetric arrangement in frequency of the multiplet, because the different $|m|$ experience a frequency shift of different size.

The non-symmetric arrangement of the components is very evident in Fig. 7. Two lines have been plotted in the middle panel, which were not shown in Fig. 6. The solid line marks the (unweighted) average frequency of the components showing non-negligible visibility. It is clearly offset, or biased, by about $0.07\,\mu$Hz, from the centroid (dotted line). The dashed line marks the actual, expected location of the "Sun-as-a-star" frequency (offset from the centroid by more than $0.1\,\mu$Hz). It differs from the unweighted average of the three visible components because the "peak bagging" procedures used to estimate the mode frequencies are influenced by the relative heights of the different m. Here, the outer $|m| = 2$ components carry greater weight in determining the fitted $l = 2$ frequency than does the weaker $m = 0$ component, thereby shifting the estimated frequency from the unweighted average.

It can be quite hard to estimate, to any reasonable accuracy and precision, the loca-
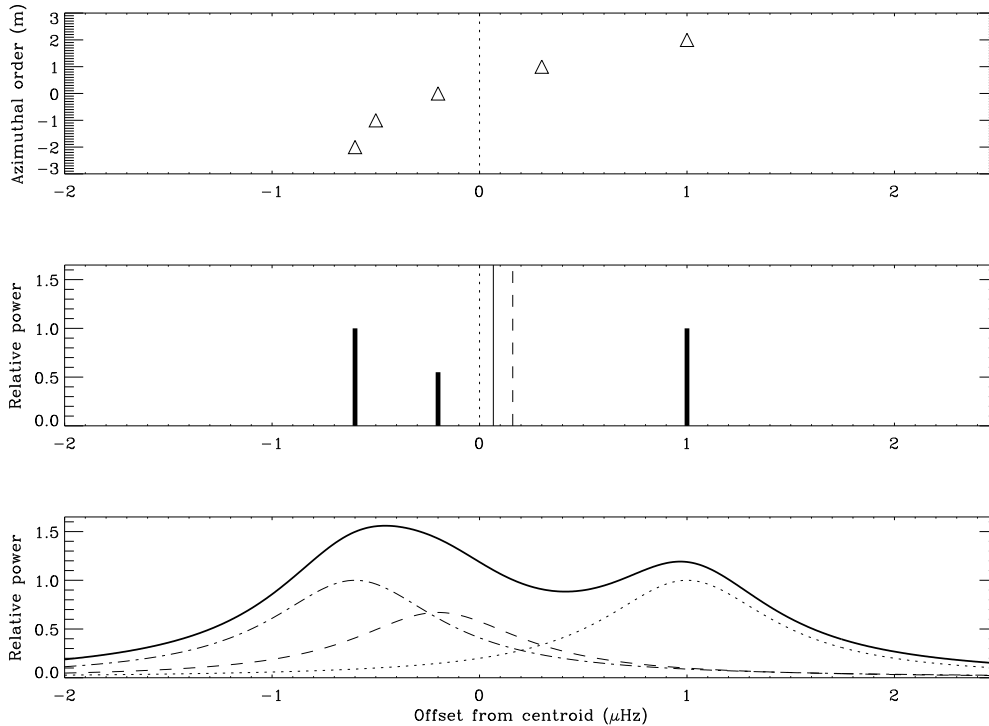
FIGURE 7. Same as Fig. 6, but during an epoch with activity levels corresponding to the maximum of a typical (modern) solar cycle. The solid and dashed lines in the middle panel mark estimates of the $l = 2$ frequency that might be derived from the Sun-as-a-star data (see text).

tions in frequency of each component individually (which, as noted above, would help to reduce the offset between the estimated frequency and the true centroid because it would be possible to compute the unweighted average frequency). Frequency estimation must contend with the fact that within the non-radial multiplets the various m lie in such close frequency proximity to one another that suitable models which seek to describe the characteristics of the m present must usually be fitted to the components simultaneously.

Is there any way to get around the problem, and in some way "correct" the Sun-as-a-star frequencies for the frequency bias? Two methods have been applied successfully. The first relies on the availability of contemporaneous resolved-Sun helioseismic data – which are sensitive to all m components – to in effect map the strength and spatial distribution of the acoustic asphericity arising from the surface activity over the epoch in question. Chaplin et al. (2004c) and Appourchaux & Chaplin (2007) show how to make the correction, using the so-called "even a coefficients" from fits to the resolved-Sun frequencies (the a coefficients are discussed later in this section). This approach is of course currently not viable for other solar-type stars. Fortunately, the second method in principle is: here, the same dataset that is used to produce the frequency estimates is also used to help calibrate the corrections that are needed to "clean" the frequencies. Implicit in the procedure is the assumption that at epochs coinciding with cycle minima, any frequency asymmetry in the mode multiplets is negligible. This assumption turns out to be reasonable for the Sun, as noted previously (Chaplin et al. 2004b).

The second method is described at length in Broomhall et al. (2009). In sum, the long dataset is divided into smaller subsets, and the frequencies of each subset are estimated.

Tried and trusted procedures are then used to measure the frequency shifts of different modes from one subset to another. The frequency shift of any given mode may be measured relative to its average frequency over the long dataset, or, for example, its frequency in the subsets (or subset) which coincide(s) with the cycle minimum (the choice has subtle consequences for propagation of the frequency uncertainties, e.g., see Chaplin et al. 2007b). It is common practice, at least for the low-l data, to average shifts over several modes to reduce uncertainties on the shifts. By making an average over many orders in n, one can track the average frequency shift from subset to subset. By making an average over a few (say two, or three) orders in n it is possible to constrain the dependence of the shifts on frequency (or n).

In the next stage of the procedure the frequency shifts are parametrized. Sun-as-a-star procedures have parametrized the shifts as a linear function of one of the global proxies of magnetic activity, the 10.7-cm radio flux (Tapping & De Tracey 1990) being a favoured choice. The mode-averaged frequency shifts are fitted to a linear function of the 10.7-cm flux (averaged over the same periods as the seismic data). This linear model then suffices to predict the expected average frequency shift for any epoch, given the 10.7-cm flux for that period. Expected shifts for individual modes are then computed using a best-fitting polynomial, which describes the measured frequency shifts as a function of frequency, relative to the average frequency shift. The predicted frequency shifts may then be subtracted from the raw frequencies (the latter measured from the full timeseries) to yield a set of corrected frequencies, commensurate with negligible surface activity. The procedure yields frequencies that are not subject to the bias discussed above, since that bias is assumed, *by definition*, to be missing at low activity.

Application of the procedure, verbatim, to other stars would of course demand that contemporaneous activity data be available (e.g., chromospheric H & K data). Such data may be hard to obtain in sufficient quantities on a large number of stars. One might instead use measures of variability in the timeseries – arising from rotational modulation of surface activity – to form a suitable proxy (Basri et al. 2010). It may instead be possible to parameterize the frequency shifts by fitting non-linear functions in time (i.e., to describe the observed shifts as functions of time), hence circumventing the need to have complementary activity data.

How large might the frequency bias be for other stars? The magnitude of the bias is governed to first order by the size of the acoustic asphericity, arising from the magnetic activity, and the angle of inclination of the star. Second-order effects come in through the interplay between the mode properties and the peak-bagging procedures used to estimate the frequencies (e.g., see discussion in Ballot et al. 2008 on correlations between different parameters).

Fig. 8 shows the predicted bias from the first-order effects. Here, we assumed an acoustic asphericity similar to that observed on the Sun, as experienced by $l = 1$ and $l = 2$ modes at the centre of the solar p-mode spectrum. The predictions therefore in principle show the bias that would be expected in the most prominent low-l modes if the Sun were to be observed at different angles of inclination, i. Two predictions are plotted in each panel. We first explain how we derived the solid-line prediction (using the $l = 2$ case as an example).

The full set of m frequencies of a mode may be described by a polynomial expansion of the form

$$\nu_{nlm} = \nu_{\text{cen}} + \sum_{j=1}^{j=2l} a_j(n,l) l \mathcal{P}_l^j(m), \tag{3.2}$$

where $\nu_{\rm cen}$ is the frequency centroid of the mode, and $\mathcal{P}_l^j(m)$ are polynomials related to the Clebsch-Gordan coefficients (Ritzwoller & Laveley 1991). An expansion of this type is commonly used to fit the frequencies observed in resolved-Sun data, where all m components are available. The even a_j describe perturbations that are non-spherically symmetric in nature, e.g., the acoustic asphericity from activity, while the odd a_j coefficients describe spherically symmetric contributions to the frequency splittings (rotation). Here, for simplicity, we assume that for the low-l modes the a_2 term dominates other terms in the description of the asphericity, and that the a_1 term dominates other terms in the description of the rotation. The required $\mathcal{P}_l^j(m)$ are:

$$\mathcal{P}_l^1(m) = m/l \tag{3.3}$$

and

$$\mathcal{P}_l^2(m) = \frac{6m^2 - 2l(l+1)}{6l^2 - 2l(l+1)}. \tag{3.4}$$

We may then write the frequencies of each of the components explicitly as:

$$\nu_{n20} = \nu_{\rm cen} - 2a_2, \tag{3.5}$$

and

$$\nu_{n21} = \nu_{\rm cen} + a_1 - a_2,$$

$$\nu_{n2-1} = \nu_{\rm cen} - a_1 - a_2, \tag{3.6}$$

and

$$\nu_{n22} = \nu_{\rm cen} + 2a_1 + 2a_2,$$

$$\nu_{n2-2} = \nu_{\rm cen} - 2a_1 + 2a_2. \tag{3.7}$$

The solid line prediction in Fig. 8 assumes that the estimated frequency of the mode is the weighted combination of the individual frequencies, where the weights are proportional to the relative heights of the components, $\mathcal{E}(i)_{lm}$ (see Equation 3.1). We weight in this way because the estimated frequency is influenced by the relative heights of the different m. We then have:

$$\nu_{n2} = \left(\sum_{m=-2}^{m=+2} \mathcal{E}(i)_{2m} \times \nu_{n2m} \right) \Big/ \left(\sum_{m=-2}^{m=+2} \mathcal{E}(i)_{2m} \right). \tag{3.8}$$

The solid lines in Fig. 8 show $\nu_{nl} - \nu_{\rm cen}$, i.e., the predicted frequency bias, as a function of i. To make the prediction we adopt $a_2 = 0.1 \, \mu$Hz (typical value at solar maximum). (The results do not depend upon a_1, which cancels when ν_{nl} is computed.)

Results on Sun-as-a-star data, and simulated asteroseismic data on solar-type stars, suggest that the weights are actually non-linear functions in $\mathcal{E}(i)_{lm}$ (e.g., see Chaplin et al. 2004b). A better description is one for which the weights are proportional to $\mathcal{E}(i)_{lm}$ raised to some positive power (four is probably a reasonable value). Here, we therefore also make predictions based upon

$$\nu_{n2} = \left(\sum_{m=-2}^{m=+2} \mathcal{E}(i)_{2m}^4 \times \nu_{n2m} \right) \Big/ \left(\sum_{m=-2}^{m=+2} \mathcal{E}(i)_{2m}^4 \right), \tag{3.9}$$

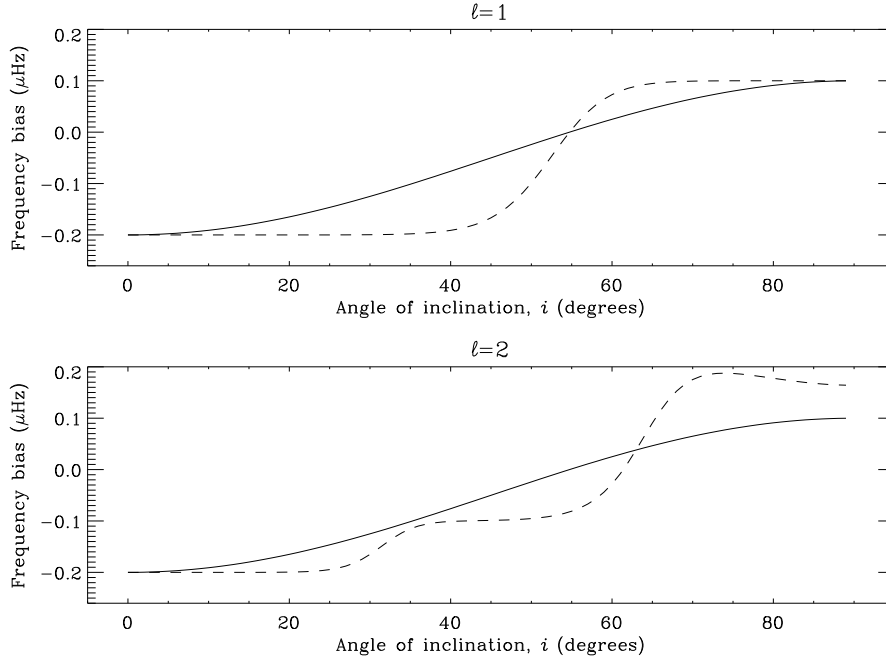which gives the dashed lines in Fig. 8.

FIGURE 8. Expected frequency bias for Sun-as-a-star observations made for different angles of inclination, i (see text for explanations of solid and dashed lines).

Equations 3.8 and 3.9 may be written in more general form (i.e., for any given l) as:

$$\nu_{nl} = \left(\sum_{m=-l}^{m=+l} \mathcal{E}(i)_{lm}^{\gamma} \times \nu_{nlm} \right) / \left(\sum_{m=-l}^{m=+l} \mathcal{E}(i)_{lm}^{\gamma} \right), \tag{3.10}$$

where γ is a constant.

The results indicate that the bias is least severe at intermediate values of i. The worst case is when $i = 0$ degrees. The non-linear weighting in $\mathcal{E}(i)_{lm}$ also changes slightly the functional form of the bias in i, e.g., in the case of $l = 1$ it extends the range of i over which the bias is more important.

When we obtain long datasets on solar-type stars, frequency uncertainties will drop to levels well below $0.1\,\mu\mathrm{Hz}$. In this context, the bias at some angles is by no means insignificant. Moreover, the bias would of course be larger on a star with higher-than-solar acoustic asphericity, i.e., one might quite reasonably expect to encounter solar-type stars where the bias may be a significant fraction of $1\,\mu\mathrm{Hz}$ or more. In sum, this source of bias in the frequencies will need to be taken into account in the not-too-distant future, if we are to avoid errors on the inferences drawn on target stars.

3.2. *Impact on frequency separation ratios*

Roxburgh & Vorontsov (2003) proposed the use for asteroseismology of the ratio of separations in frequency between low-l p-modes: *Frequency separation ratios* are formed from the large and small frequency separations of the p modes,

$$\Delta\nu_l(n) = \nu_{nl} - \nu_{n-1,l}, \tag{3.11}$$

and

$$d_{l\,l+2}(n) = \nu_{n,l} - \nu_{n-1,l+2}. \tag{3.12}$$

Data on modes in the range $0 \leq l \leq 3$ may be used to make ratios, according to:

$$r_{02}(n) = \frac{d_{02}(n)}{\Delta\nu_1(n)}, \qquad r_{13}(n) = \frac{d_{13}(n)}{\Delta\nu_0(n+1)}. \tag{3.13}$$

Roxburgh & Vorontsov used an asymptotic method to show that the ratios are very insensitive to conditions in the near-surface layers of a solar-type star. This is an attractive property since the outer layers are uncertain and hard to model accurately. As such, the ratios in principle offer a clean diagnostic of the internal properties of a star (see also Otí Floranes et al. 2005 and Roxburgh 2005). They are nevertheless potentially sensitive to the acoustic asphericity – as was pointed out by Otí Floranes et al. (2005), and discussed at length by Chaplin et al. (2005) – which is clearly undesirable if one wishes to suppress any signatures from the near-surface layers.

That the ratios are sensitive to the solar cycle may be understood as follows. For the Sun-as-a-star data, measured frequency shifts of the $l = 2$ modes are larger than those of the neighbouring $l = 0$ modes (because the frequencies of these modes are dominated by the $|m| = 2$ components, which are more sensitive to the acoustic perturbations arising in the active latitudes than are the $l = 0$ modes). The measured $d_{l\,l+2}(n)$ will therefore carry a residual signature of the solar cycle, being smaller at higher levels of activity. Residual solar-cycle changes in $\Delta\nu_l(n)$ are, fractionally, much smaller (but nevertheless measurable; see Broomhall et al. 2011), so that in the case of, for example, $r_{02}(n)$:

$$\delta r_{02}(n)/r_{02}(n) \simeq \delta d_{02}(n)/d_{02}(n). \tag{3.14}$$

For the Sun-as-a-star data, $\delta d_{02}(n)/d_{02}(n) \approx -0.01$ for modes at the centre of the p-mode spectrum observed at solar maximum, hence, we would expect the ratios to decrease between solar minimum and solar maximum by about this amount. Fig. 9 plots measured fractional differences in r_{02}, as averaged over the most prominent low-l modes. The differences were computed between two BiSON Sun-as-a-star datasets, one formed of from around solar maximum, the other formed of data from around solar minimum.

The potential impact on observations of other solar-type stars will depend upon both the nature of the near-surface magnetic fields, and also the angles of inclination offered by the stars. In Section 4 below, we shall develop a simple model of the frequency shifts that will allow us to make these predictions for other stars. We therefore return in that section to the frequency separation ratios.

3.3. *Impact on shapes of resonant peaks*

What effect will stellar-cycle shifts in frequency through a long timeseries have on the underlying shapes of the p-mode peaks, when those peaks are observed in frequency-power spectra made from the full timeseries? Given a significant shift, one would expect the Lorentzian-like peak shapes to be distorted, with the mode power being spread out in frequency thereby flattening the profiles. Whether or not a frequency shift $\delta\nu$ is significant in this context is determined by the ratio

$$\epsilon = \delta\nu/\Delta, \tag{3.15}$$

i.e., the ratio of the shift to the linewidth of the mode. The larger this ratio, the more distorted a mode peak will be.

Chaplin et al. (2008b) derived analytical descriptions of the distorted peak profiles. Since for solar-type stars we expect the modes to be excited and damped on timescales much shorter than that on which any significant change of the mode frequencies is observed, the profiles may be assumed to correspond to the average of all the instantaneous profiles taken at any time t within the full period of observation T. Each instantaneous
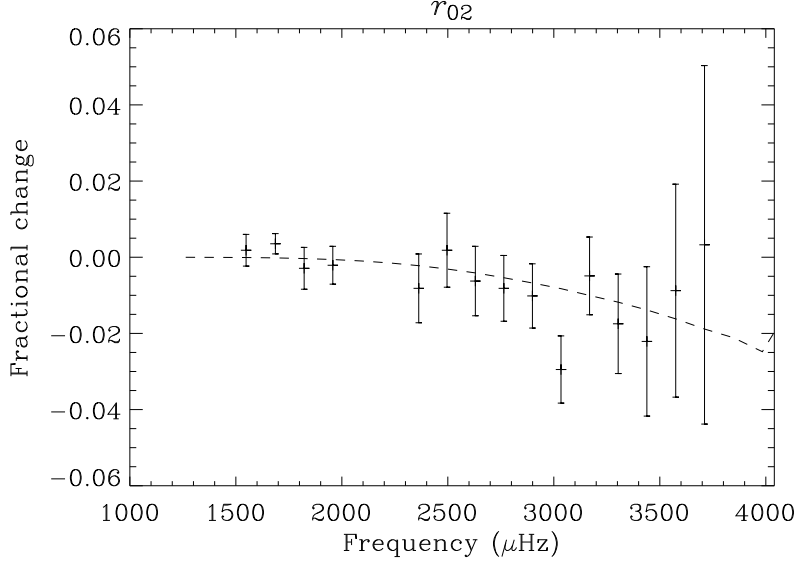
FIGURE 9. Fractional change in r_{02} – as averaged over the most prominent low-l modes – between two BiSON Sun-as-a-star datasets, one around solar maximum and one around solar minimum (differences in sense maximum minus minimum). (From Chaplin et al. 2005.)

profile may be described as, for example, a Lorentzian with a central frequency $\nu(t)t$, such that the time-averaged profile is

$$\langle P(\nu) \rangle = \frac{1}{T} \int_0^T \frac{H}{1 + \left(\frac{\nu - \nu(t)}{\Delta/2} \right)^2} \, dt, \tag{3.16}$$

where the angled brackets indicate an average over time, and H and Δ are the mode height (maximum power spectral density) and linewidth, respectively.

Chaplin et al. (2008b) derived profiles given by two functions describing the frequency shifts in time: first, the simplest possible function, this being a linear variation over time (which would be relevant for describing the profiles given by observations made on the steepest parts of the rising or falling phases of a stellar cycle); and second, a co-sinusoidal variation, to mimic a full stellar cycle. They neglected the effects of the solar-cycle variations in mode power, height and width.

A simple linear variation in time may be described by

$$\nu(t) = \nu_0 + \delta\nu \frac{t}{T}, \tag{3.17}$$

where ν_0 is the unperturbed frequency, and the frequency is shifted by an amount $\delta\nu$ from the start $(t = 0)$ to the end $(t = T)$ of the timeseries. Substitution of Equation 3.17 into Equation 3.16, followed by solution of the integral, gives the predicted mode profile:

$$\langle P(\nu) \rangle = \frac{H}{2\epsilon} \mathrm{atan} \left(\frac{2\epsilon}{1 - \epsilon^2 + X^2} \right), \tag{3.18}$$

where ϵ is the shift-to-linewidth ratio (Equation 3.15), and

$$X = \frac{\nu - (\nu_0 + \delta\nu/2)}{\Delta/2}. \tag{3.19}$$

The top panel of Figure 10 shows profiles given by Equation 3.18. The unperturbed profile (solid line) is for a mode having an unperturbed frequency of $\nu_0 = 3000\,\mu\text{Hz}$, an unperturbed linewidth of $\Delta = 1\,\mu\text{Hz}$, and an unperturbed height of $H = 100$ units. The other curves show the profiles that result when the frequency shift, $\delta\nu$, is: $0.15\,\mu\text{Hz}$ (dotted line); $0.40\,\mu\text{Hz}$ (dashed line); $1.50\,\mu\text{Hz}$ (dot-dashed line); and $3.0\,\mu\text{Hz}$ (dot-dot-dot-dashed line). Since $\Delta = 1\,\mu\text{Hz}$, the $\delta\nu$ also correspond to the shift-to-linewidth ratios, ϵ. To put the values in context, we once more recall that low-l solar p modes at $\approx 3000\,\mu\text{Hz}$, which also have width $\approx 1\,\mu\text{Hz}$, and show a frequency shift of approximately $0.40\,\mu\text{Hz}$ from the minimum to the maximum of the solar activity cycle.

Only at the two largest shifts (dot-dashed and dot-dot-dot-dashed lines) do the profiles depart appreciably from the Lorentzian form. Closer inspection of the profiles does reveal some modest distortion at the two, smaller, Sun-like shifts. These have $\epsilon = 0.15$ and 0.40 respectively.

A co-sinusoidal variation of the mode frequency may be described by

$$\nu(t) = \nu_0 + \frac{\Delta\nu}{2}\left[1 - \cos\left(\frac{2\pi t}{P_{\text{cyc}}}\right)\right], \tag{3.20}$$

where ν_0 is again the unperturbed frequency (i.e., the frequency at minimum activity), while $\delta\nu$ is now the full amplitude (from minimum to maximum) of the cyclic frequency shift (not the *total* shift, as in the linear model). When the length of observation, T, equals the cycle period P_{cyc} (or one-half of the period), the average profile resulting from Equation 3.20 is:

$$\langle P(\nu)\rangle = \frac{\sqrt{L_1.L_2}}{\sqrt{1 - \epsilon^2.F(L_1, L_2)}}, \tag{3.21}$$

where

$$F(L_1, L_2) = \frac{4L_1 L_2}{H\left(\sqrt{L_1} + \sqrt{L_2}\right)^2},$$

$$L_1 = \frac{H}{1 + (X - \epsilon)^2},$$

$$L_2 = \frac{H}{1 + (X + \epsilon)^2},$$

$$X = \frac{\nu - (\nu_0 + \frac{\delta\nu}{2})}{\Delta/2}.$$

Since the frequency spends more time around its maximum and minimum values, power near these extreme frequencies will have more weight in the time-averaged profile, giving the profile a double-humped appearance. This is reflected in the analytical expression through the two Lorentzians L_1 and L_2. It is obvious from Equation 3.21 that when $\epsilon \ll 1$ the profile tends to a single Lorentzian.

The bottom panel of Figure 10 shows predicted profiles from Equation 3.21†, assuming observations made over a complete activity cycle, and with the same shifts $\delta\nu$ as were applied in the linear-model case (top panel of Figure 10). As for the simpler linear variation, it is only at the two largest $\delta\nu$ that the profiles depart appreciably from the unperturbed (Lorentzian) form, here showing the predicted "humps" at the extreme frequencies of the cycle. However, closer inspection again reveals some distortion of the

† Versions of Equations 3.18 and 3.21, which allow for the small amounts of peak asymmetry observed in real solar p modes, are presented in Chaplin et al. (2008). We note here that this asymmetry is negligible for modes at the centre of the solar p-mode spectrum.
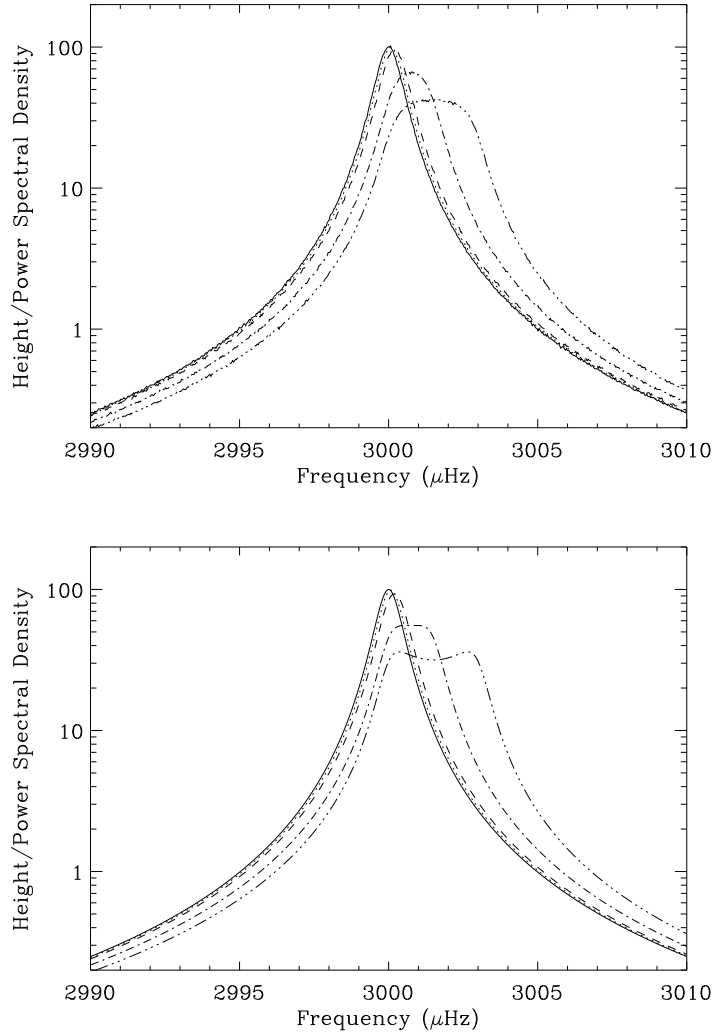
FIGURE 10. Top panel: Peak profiles expected for a single mode of width $\Delta = 1\,\mu$Hz in the frequency-power spectrum of a time series within which the frequency was varied in a linear manner by total amount $\delta\nu$. Various linestyles are: no shift (solid line); $\delta\nu = 0.15\,\mu$Hz (dotted line); $0.40\,\mu$Hz (dashed line); $1.50\,\mu$Hz (dot-dashed line); and $3.0\,\mu$Hz (dot-dot-dot-dashed line). Bottom panel: Peak profiles expected for a single mode of the same width, but where the frequency has instead been subjected to a co-sinusoidal variation in time. The timeseries is assumed to have length equal to one cycle period; while the amplitude of the cycle is $\delta\nu/2$ (giving a total minimum-to-maximum shift in frequency of $\delta\nu$). Linestyles are as per the upper panel. (From Chaplin et al. 2008b.)

Lorentzian shapes at the small Sun-like shifts. For a given shift, this distortion appears to be slightly larger than in the simpler, linear case.

While the distortion seen at the Sun-like shifts is evidently modest, Chaplin et al. (2008b) showed that it is nevertheless just detectable in long, multi-year Sun-as-a-star datasets. By fitting modes to the usual Lorentzian-like models – which do not allow for the distortion – rather than modified models, like the ones shown above, Chaplin et al.

showed that an overestimation (underestimation) of the linewidth (height) parameter results. This bias is estimated to be of size comparable to the observational uncertainties given by datasets of length several years. Bias in the frequency parameter is much less of an issue.

The distortion may of course be more important for asteroseismic datasets on some solar-type stars, e.g., those for which the ratio of the stellar-cycle frequency shifts to the mode linewidths is larger than for the Sun. The shifts need only be about twice as strong as those on the Sun before significant distortion of the peaks results. Visible distortion of the mode profiles in asteroseismic data may as such provide an initial diagnostic of strong stellar-cycle signatures over the duration of the observations.

4. Estimated frequency shifts, and inference on spatial distribution of surface activity

We have seen that near-surface activity that is distributed in a non-spherically symmetric manner (i.e., the aforementioned acoustic asphericity) will give rise to differences in the magnitudes of the frequency shifts of modes of different $(l, |m|)$. For a scenario like that on the Sun, where bands of strong magnetic activity are located at lower latitudes, it will be the sectoral components of the non-radial modes that show the largest shifts. As was noted in Section 3.1, these components, for which $l = |m|$, have more sensitivity to changes at lower latitudes than do their zonal counterparts. It is possible to measure differences in the sizes of the frequency shifts of the different low-l modes (e.g., see Chaplin et al. 2004a; Jiménez-Reyes 2004). If such measurements could be made on other stars, might it not then be possible to make some inference on the surface distribution in latitude of the activity, from measurement of the relative sizes of the frequency shifts (assuming, as mentioned elsewhere, that it is near-surface perturbations that are the dominant cause of the observed shifts)?

This question was considered by Chaplin et al. (2007a). They used a very simple model of the spatial distribution of the surface activity on a solar-type star, in which the activity was given a uniform amplitude between some lower and upper bounds in latitude, λ. As should be evident from what follows, it would be very straightforward to incorporate a more sophisticated model of the activity. They used this model to predict expected frequency shifts of modes of different $(l, |m|)$. Here, we reproduce their model, and use it to show explicitly how it might be used with results on observed frequency shifts to make inference on the active latitudes of a star. Before that, we use its predictions to show how estimated *average* frequency shifts, and estimated frequency separation ratios, of solar-type stars are affected by the angle of inclination.

Implicit in the calculation of the expected frequency shifts is the assumption that contributions to the fractional change in the sound speed are non-zero only very close to the surface. Consideration of the radial dependence of the sound speed is neglected (again, to simplify the description). The expected shifts, $\delta\nu_{lm}$ are then proportional to (e.g., Moreno-Insertis & Solanki 2000)

$$\delta\nu_{lm} \propto \left(l + \frac{1}{2}\right) \frac{(l-m)!}{(l+m)!} \int_0^\pi |P_l^m(\cos\theta)|^2 B(\theta) \sin\theta \, \mathrm{d}\theta, \qquad (4.1)$$

where the $P_l^m(\cos\theta)$ are Legendre polynomials, and $B(\theta)$ describes the distribution in co-latitude θ of the activity. (Note that $\lambda = 90 \, \mathrm{degrees} - \theta$.) Chaplin et al. calibrated the model so that for a Sun-like configuration the predicted $\delta\nu_{00}$ was equal to the observed average shift of the solar $l = 0$ modes. This calibration was subsumed within the $B(\theta)$, as discussed below. For all surface configurations tested, the activity at cycle minimum
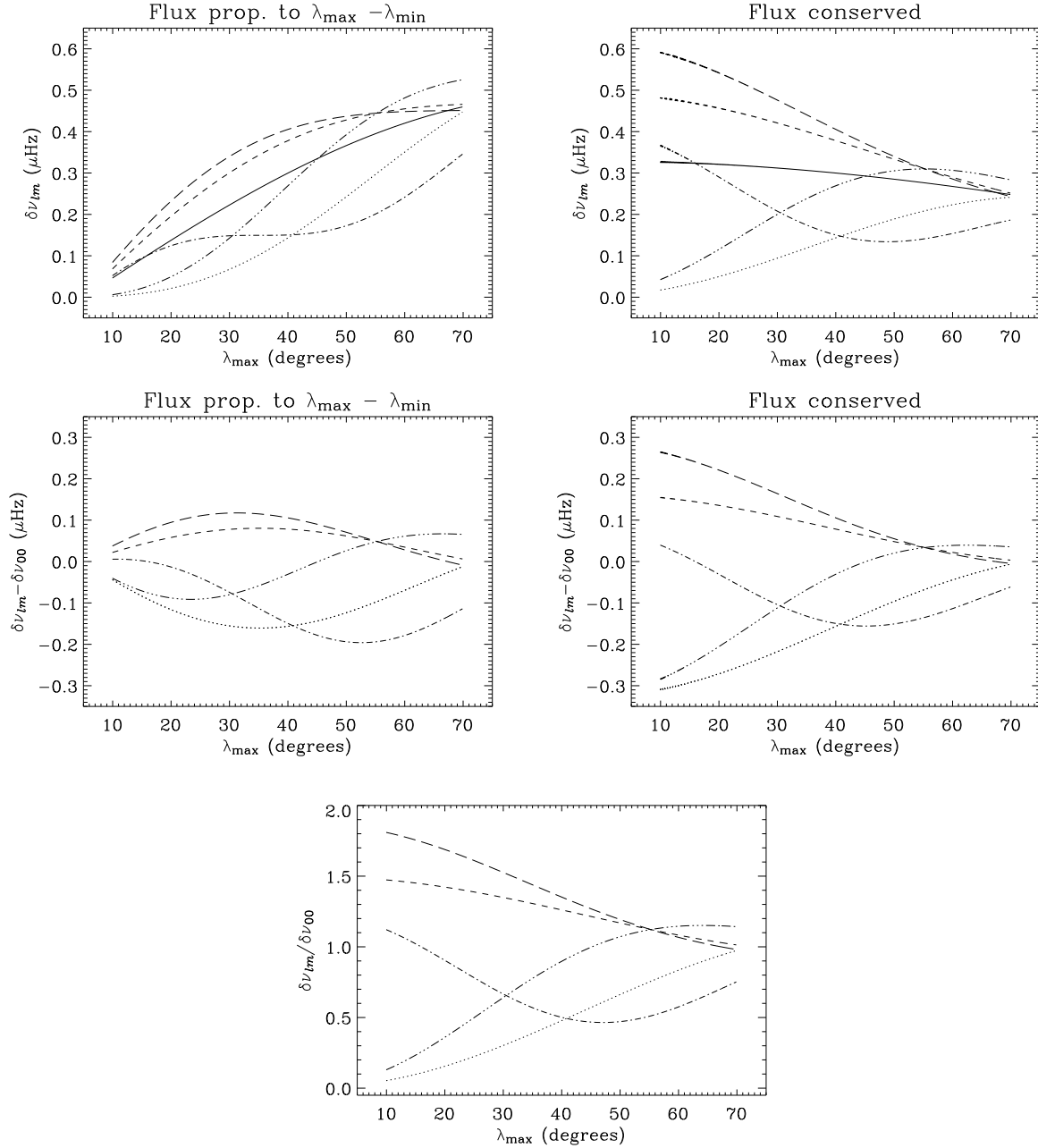
FIGURE 11. Frequency shifts given by a simple model of stellar surface magnetic activity (magnetic flux). Linestyles, which are the same in all panels, show results for different $(l, |m|)$ components as follows: solid for $(0,0)$; dotted for $(1,0)$; short dashes for $(1,1)$; dot-dashed for $(2,0)$; dot-dot-dot-dashed for $(2,1)$; and long dashes for $(2,2)$. Top panels: shifts calculated from models based on Equation 4.2 (left-hand panel) and Equation 4.3 (right-hand panel). Middle panels: residuals given by subtracting the $(0,0)$ shifts from the other component shifts. Bottom panel: ratio of component shifts to $(0,0)$ shifts (these ratios are the same for both sequences of models). (From Chaplin et al. 2007a.)

was set to $B(\theta) = 0$. Values of $\delta\nu_{lm}$ determined at the simulated cycle maxima therefore corresponded to the sought-for stellar cycle shifts.

In a first sequence of models $B(\theta)$ was set to some constant value at cycle maximum. This value was the same for *all* model configurations. The only parameter that was changed from model to model, and therefore the only factor that could alter the observed shifts, was the maximum latitude of the activity, $\lambda_{\max}$. The minimum latitude was fixed for all models at $\lambda_{\min} = 5$ degrees. In summary:

$$B(\theta) = \begin{cases} \text{const} & \text{for } \lambda_{\min} \leq |\lambda| \leq \lambda_{\max}, \\ 0 & \text{otherwise.} \end{cases} \qquad (4.2)$$

In the scenario above, the total surface magnetic flux is proportional to $\lambda_{\max} - \lambda_{\min}$, and therefore varied by over an order of magnitude for the range of computations made ($10 \leq \lambda_{\max} \leq 70$ degrees). Chaplin et al. also made a second sequence of models in which the total flux was conserved for all values of $\lambda_{\max}$. This model is described by:

$$B(\theta) = \begin{cases} \text{const}/\left(\lambda_{\max} - \lambda_{\min}\right) & \text{for } \lambda_{\min} \leq |\lambda| \leq \lambda_{\max}, \\ 0 & \text{otherwise.} \end{cases} \qquad (4.3)$$

Chaplin et al. used results from Knaack et al. (2001) to help guide their calibration of Equations 4.2 and 4.3. Knaack et al. noted that observations of the surface activity during the cycle 22 maximum showed sunspots confined to bands from 5 to 30 degrees, and faculae in bands from 5 to 40 degrees. On the Sun, faculae occupy a much larger surface area than the spots (see also De Toma et al. 2004). The constant in Equations 4.2 and 4.3 was therefore calibrated so that when $\lambda_{\max} = 40$ degrees, the calculated shift of the radial modes was $\delta\nu_{00} \sim 0.3\,\mu$Hz. This is the value observed for the most prominent low-l radial modes of the Sun.

The top two panels of Fig. 11 show the calibrated shifts from both sequences of models, based on Equation 4.2 (left-hand panel) and Equation 4.3 (right-hand panel). The middle panels show residuals given by subtracting the $(l, |m|) = (0,0)$ shifts from the other component shifts. The bottom panel shows the ratio of the component shifts and the $(0,0)$ shifts: since $B(\theta) = \text{const.}$ for both sequences of models, the ratios are also the same (hence only one plot).

Let us first consider the impact of the angle of inclination, i, on estimated *average* frequency shifts for solar-type stars. We again adopt the approach of Section 3.1, to take into account the effect of the relative visibility of components within any given l (Equations 3.8 to 3.10). We take the frequency shifts $\delta\nu_{lm}$ predicted by the simple model in this section, for different angles of inclination, i (as computed assuming the solar calibration). Since the $\delta\nu_{lm}$ are functions of i, we write $\delta\nu_{lm}(i)$. We weight the shifts of each component within a multiplet, to give the effective (weighted average) shift at that l:

$$\delta\nu_l = \left(\sum_{m=-l}^{m=+l} \mathcal{E}(i)_{lm}^{\gamma} \times \delta\nu_{lm}\right) \Big/ \left(\sum_{m=-l}^{m=+l} \mathcal{E}(i)_{lm}^{\gamma}\right), \qquad (4.4)$$

Since one may then choose to average results over different l, to reduce errors, we compute a final, weighted average shift according to:

$$\langle \delta\nu \rangle = \left(\sum_{l=0}^{l=2} \mathcal{E}_l' \times \delta\nu_{lm}\right) \Big/ \left(\sum_{l=0}^{l=2} \mathcal{E}_l'\right), \qquad (4.5)$$
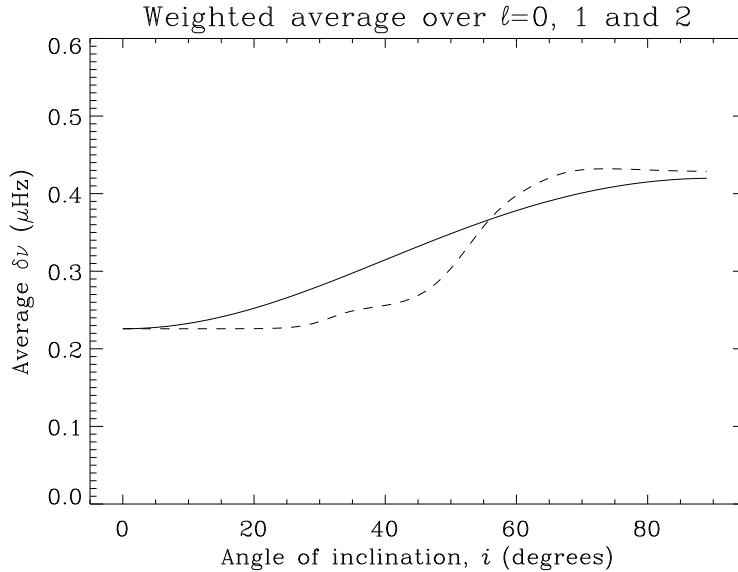
Weighted average over ℓ=0, 1 and 2

FIGURE 12. Predicted frequency shift, averaged over $l = 0$, 1 and 2 modes, as a function of angle of inclination, i, assuming a solar-like spatial distribution of surface activity (see text for details).

using the predictions for $l = 0$, 1 and 2. Here, the $\mathcal{E}'_l$ are the relative total l visibilities, which we take to be 1, 1.5 and 0.5 (for $l = 0$, 1 and 2, respectively).

Fig. 12 plots the $\langle\delta\nu\rangle$ as a function of i, for $\gamma = 1$ (solid line) and $\gamma = 4$ (dashed lines). When i is low, the $m = 0$ components have the highest visibility in the $l = 1$ and $l = 2$ modes, which reduces the size of the average frequency shift (since these components show smaller shifts than the other components when $\lambda_{\mathrm{max}} = 40$ degrees). The plot shows clearly that for a solar-like spatial distribution of surface activity, estimated average frequency shifts could differ by up to a factor of two, depending upon the angle i. It will clearly be important to have good constraints on i in order to properly interpret measured frequency shifts of solar-type stars (e.g., see Ballot et al. 2006, 2008).

We also use predictions from Equation 4.4 above to show the impact of i on the observed frequency separation ratios. Fig. 13 plots the implied fractional change, between solar minimum and maximum, in the frequency separation ratios r_{02} of the most prominent solar p modes. Recall from Section 3.2 that results from BiSON data give a fractional change of -0.01; this is consistent with the prediction shown here for $i = 90$ degrees. Fig. 13 shows that for the Sun the largest offset occurs at $i = 0$ degrees, when the predicted fractional change is 0.02 (positive). Since we should expect to observe solar-type stars with larger acoustic asphericity than the Sun, it is possible that bias in the frequency separation ratios could reach levels of several per cent.

Let us now use the frequency shift *ratios* plotted in the bottom panel of Fig. 11, together with results on measured frequency shifts of low-l solar p modes, to make an estimate of λ_{max} for the Sun. By using the ratios as opposed to the absolute values of the shifts we remove any dependence of the result on the absolute calibration of the model shifts. Let us denote the shift ratios by $k_{lm} = \delta\nu_{lm}/\delta\nu_{00}$. From the BiSON Sun-as-a-star data in Chaplin et al. (2004a), we may infer observed ratios of $k_{11} = 1.23 \pm 0.14$ and $k_{22} = 1.45\pm016$. (The observed $l = 2$ Sun-as-a-star shifts will include a contribution from the (2,0) components, however the contribution is relatively weak, and the observed shifts
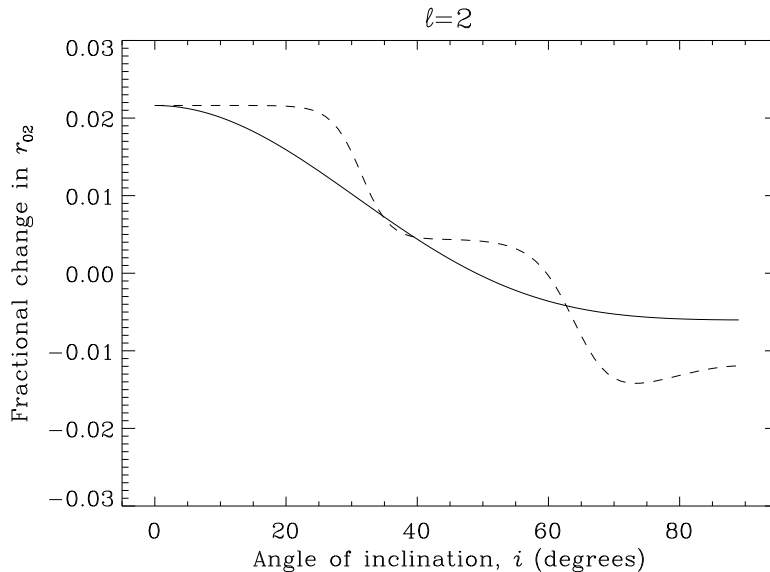
FIGURE 13. Predicted fractional change (from solar minimum to solar maximum) in frequency separation ratios r_{02} of the most prominent solar p modes, as a function of angle of inclination, i, assuming a solar-like spatial distribution of surface activity (see text for details).

may be regarded, to very good approximation, as being those of the (2,2) components.) To infer $\lambda_{\max}$, we use the appropriate curves from Fig. 11. Uncertainties in $\lambda_{\max}$ follow from

$$\delta\lambda_{\max} = \frac{\Delta\lambda_{\max}}{\Delta k_{lm}}\delta k_{lm}, \tag{4.6}$$

where δk_{lm} are the observed uncertainties in the k_{lm}, and $\Delta\lambda_{\max}/\Delta k_{lm}$ are the gradients of the respective curves in the vicinity of k_{lm}. From the $l = 1$ shift ratio we find $\lambda_{\max} = 43 \pm 16$ degrees, and from the $l = 2$ shift ratio we find $\lambda_{\max} = 34 \pm 10$ degrees. These values are of course reasonable estimates for the Sun.

One may adopt a similar procedure using asteroseismic data on other solar-type stars. One would again need to have good constraints on i, which may be obtained from peak-bagging of the modes in the frequency-power spectrum.

5. How long will it take to detect evolutionary changes?

We finish by thinking longer-term, and ask whether it might be possible to measure evolutionary changes in solar p-mode frequencies, using low-l data (the choice of data again made with other solar-type stars in mind).

First, consider the precision in the estimated frequencies. We take the estimated uncertainties, σ_{nl}, from Broomhall et al. (2009), who measured low-l frequencies in 8640 d (23.7 yr) of BiSON Sun-as-a-star data. The published list included 81 frequencies, covering $l = 0$ to 3. An estimate of the *combined* precision in *all* the measured frequencies, $\langle\sigma\rangle$, is given by:

$$\langle\sigma\rangle = \left(\sum_{nl} 1/\sigma_{nl}^2\right)^{-1/2} \simeq 1.1\,\text{nHz}. \tag{5.1}$$

We may then estimate the combined precision, $\sigma_{\Delta t}$, for any dataset length, Δt (in yr)
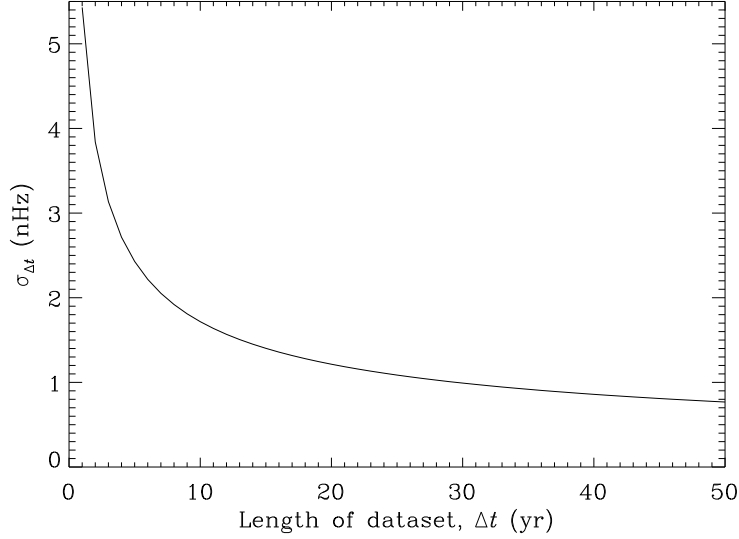
FIGURE 14. Combined frequency precision, $\sigma_{\Delta t}$, for low-l observations, extrapolated to different dataset lengths, Δt (see text for more details).

from:

$$\sigma_{\Delta t} = \left(\frac{8640}{365}\right)^{1/2} \langle\sigma\rangle \, \Delta t^{-1/2} \simeq 5.4 \, \Delta t^{-1/2} \, \mathrm{nHz}, \qquad (5.2)$$

since the frequency uncertainties of the observed modes are expected to scale with the square root of time. Fig. 14 plots $\sigma_{\Delta t}$ as a function of dataset length, Δt.

How do the $\sigma_{\Delta t}$ compare to the expected frequency shifts from evolutionary effects? Those shifts should, to good approximation, be dominated by the slow expansion in radius of the Sun as it evolves on the main sequence. Since, to first order, the frequencies scale like the square root of the mean density of the star, we have:

$$\left(\frac{\delta\nu}{\nu}\right) \simeq \frac{1}{2}\left(\frac{\delta\rho}{\rho}\right) \simeq -\frac{3}{2}\left(\frac{\delta R}{R}\right). \qquad (5.3)$$

This implies that

$$\frac{1}{\nu}\left(\frac{\delta\nu}{\delta t}\right) \simeq -\frac{3}{2R}\left(\frac{\delta R}{\delta t}\right). \qquad (5.4)$$

Fig. 15 plots $1/\nu(\delta\nu/\nu)$, as determined from the frequencies of several stellar evolutionary models (Yale-Yonsei models) made with solar mass and solar composition, but with varying ages ranging $\pm 0.02\,\mathrm{Gyr}$ about the accepted solar age. The different linestyles show results for different l ($l = 0$ as a thin solid line, $l = 1$ as a dotted line, $l = 2$ as a dashed line, and $l = 3$ as a dot-dashed line). The thick grey line plots $-(3/2R)(\delta R/R)$, as determined from the radii of the stellar models. It has a value $-5.3 \times 10^{-11}\,\mathrm{yr}^{-1}$, which agrees quite well with the estimated gradient from the model-computed frequencies, verifying that the frequencies scale in an approximately homologous fashion.

We may then estimate to good approximation the expected evolutionary frequency shift $\Delta\nu_{nl}$ of a mode over a length of time Δt (in yr):

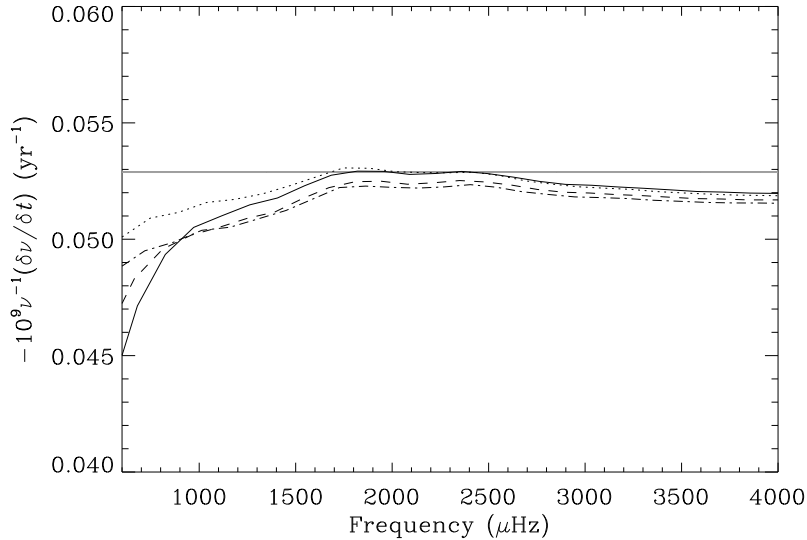$$\Delta\nu_{nl} \simeq -5.3 \times 10^{-11} \nu_{nl} \Delta t. \qquad (5.5)$$

FIGURE 15. $\nu(\delta\nu/\nu)$, as determined from the frequencies of several stellar evolutionary models made with solar mass and solar composition, but with varying ages, ranging $\pm 0.02\,\text{Gyr}$ about the accepted solar age. Linestyles show data for $l = 0$ (thin solid line), $l = 1$ (dotted line), $l = 2$ (dashed line) and $l = 3$ (dot-dashed line). The thick grey line plots $-(3/2R)(\delta R/R)$, as determined from the radii of the stellar models.

For a mode at the centre of the solar p-mode spectrum, having a frequency $\approx 3000\,\mu\text{Hz}$, we obtain $-1.6 \times 10^{-4}\,\text{nHz}$ in $1\,\text{yr}$, and $-1.6 \times 10^{-2}\,\text{nHz}$ in $100\,\text{yr}$. These expected shifts are significantly smaller than the combined uncertainties expected for each length, being just over $5\,\text{nHz}$ in $1\,\text{yr}$, and about $0.5\,\text{nHz}$ in $100\,\text{yr}$. The shift and combined uncertainty have similar sizes only when $\Delta t \approx 1100\,\text{yr}$.

REFERENCES

Anguera Gubau, M., Pallé, P. L., Perez Hernandez, F., Régulo, C. & Roca-Cortés, T., 1992, A&A, 255, 363

Appourchaux, T., 1998, in: Structure and Dynamics of the Interior of the Sun and Sun-like Stars SOHO 6/GONG 98 Workshop Abstract, June 1-4, 1998, Boston, Massachusetts, p. 37

Appourchaux, T., Michel, E., Auvergne, M., et al. 2008, A&A, 488, 705

Appourchaux, T., Chaplin, W. J., 2007, A&A, 469, 1151

Ballot, J., García, R. A., Lambert, P., 2006, MNRAS, 369, 1281

Ballot, J., Appourchaux, T., Toutain, T., Guittet, M., 2008, A&A, 486, 867

Basri, G., Walkowicz, L. M., Batalha N., et al., 2010, ApJ, 713, L155

Basu, S., Mandel, A., 2004, ApJ, 617, L155

Böhm-Vitense, E., 2007, ApJ, 657, 486

Broomhall, A.-M., Chaplin, W. J., Elsworth, Y., Fletcher, S. T., New, R., 2009, ApJ, 700, 162L

Broomhall, A.-M., Chaplin, W. J., Elsworth, Y., New, R., 2011, MNRAS, in the press

Chaplin, W. J., Elsworth, Y., Isaak, G. R., Lines, R., McLeod, C. P., Miller, B. A., New, R., 1998, MNRAS, 300, 1077

Chaplin, W. J., Appourchaux, T., Elsworth, Y., Isaak, G. R., Miller, B. A. & New, R., 2000, MNRAS, 314, 75

Chaplin, W. J., Appourchaux, T., Elsworth, Y., Isaak, G. R., New, R., 2001, MNRAS, 324, 910

Chaplin, W. J.: 2004, in: SOHO 14/GONG 2004, 'Helio- and Asteroseismology: Toward and Golden Future', ed. D. Dansey, ESA SP-559, Noordwijk, Netherlands, 34

Chaplin, W. J., Elsworth, Y., Isaak, G. R., Miller, B. A., New, R., 2004a, MNRAS, 352, 1102

Chaplin W. J., Appourchaux T., Elsworth Y., Isaak G. R., Miller B. A., New R., 2004c, A&A, 424, 713

Chaplin W. J., Appourchaux T., Elsworth Y., Isaak G. R., Miller B. A., New R., Toutain, T., 2004b, A&A, 416, 341

Chaplin, W. J., Elsworth, Y., Miller, B. A., New, R., Verner, G. A., 2005, ApJ, 635, 105

Chaplin, W. J., Elsworth, Y., Houdek, G., New, R., 2007a, MNRAS, 377, 17

Chaplin, W. J., Elsworth, Y., Miller, B. A., New, R., Verner, G. A., 2007b, ApJ, 659, 1749

Chaplin, W. J., Houdek, G., Appourchaux, T., Elsworth, Y., New, R., Toutain, T., 2008a, A&A, 483, 43

Chaplin, W. J., Elsworth, Y., New, R., Toutain, T., 2008b, MNRAS, 384, 1668

Chaplin, W. J., Appourchaux, T., Elsworth, Y., et al., 2010, ApJ, 713, L169

Christensen-Dalsgaard J., Berthomieu G., 1991, in: Solar Interior and Atmosphere, eds. A. N. Cox, W. C. Livingston, M. Matthews, Tucson, University of Arizona Press, p. 401

De Toma G., White O. R., Chapman G. A., Walton S. R., Preminger D. G., Cookson A. M., 2004, ApJ, 609, 1140

Elsworth, Y., Howe, R., Isaak, G. R., McLeod, New, R., 1990, Nat, 345, 322

Elsworth, Y., Howe, R., Isaak, G. R., McLeod, Miller, B. A., New, R., Speake, C. C., Wheeler, S. J., 1994, ApJ, 434, 801

Dziembowski, W. A., Goode, P. R., 2005, ApJ, 625, 548

Fletcher, S. T., Broomhall, A.-M., Salabert, D., Basu, S., Chaplin, W. j., Elsworth, Y., García, R. A., New, R., 2010, ApJ, 718, L19

García, R. A., Mathur, S., Salabert, D., Ballot, J., Régulo, C., Metcalfe, T. S., Baglin, A., 2010, Sci, 329, 1032

Gelly B., Lazrek M., Grec G., Ayad A., Schmider F. X., Renaud C., Salabert D., Fossat E., 2002, A&A, 394, 285

Gilliland, R. L., Brown, T. M., Christensen-Dalsgaard, J., et al., 2010, PASP, 122, 131

Gizon, L., Solanki, S. K., 2003, ApJ, 589, 1009

González-Hernández, I., Howe, R., Komm, R., Hill, F., 2010, ApJ, 713, L16

Gough, D. O., 1990, in: Progess of Seismology of the Sun and Stars, Proceedings of the Oji International Seminar Held at Hakone, Japan, eds. Y. Osaki, H. Shibahashi, Lecture Notes in Physics, vol. 367 (Springer-Verlag), p. 283

Howe, R., Komm, R. W., Hill, F., 2002, ApJ, 580, 1172

Howe, R., Christensen-Dalsgaard, J., Hill, F., Komm, R., Schou, J., Thompson, M. J., 2009, ApJ, 701, L87

Houdek, G., Chaplin, W. J., Appourchaux, T., Christensen-Dalsgaard, J., Däppen, W., Elsworth, Y., Gough, D. O., Isaak, G. R., New, R., Rabello-Soares, M. C., 2001, MNRAS, 327, 483

Jiménez-Reyes, S. J., Régulo, C., Pallé, P. L., Roca-Cortés, T., 1998, A&A, 329, 1119

Jiménez-Reyes, S. J., Corbard, T., Pallé P. L., Roca-Cortés, T., Tomczyk, S., 2001, A&A, 379, 622

Jiménez-Reyes, S. J., García, R. A., Chaplin, W. J., Korzennik, S. G., 2004, ApJ, 610, 65

Jiménez-Reyes, S. J., Chaplin, W. J., Elsworth, Y., García, R. A., Howe, R., Socas-Navarro, H., Toutain, T., 2007, ApJ, 604, 1135

Karoff, C., Metcalfe, T. S., Chaplin, W. J., Elsworth, Y., Kjeldsen, H., Arentoft, T., Buzasi, D., 2009, MNRAS, 399, 914

Knaack R., Fligge M., Solanki S. K., Unruh Y. C., 2001, A&A, 376, 1080

Komm, R., Howe, R., Hill, F., 2000, ApJ, 531, 1094

Libbrecht, K. G., Woodward, M. F., 1990, Nat, 345, 779

Metcalfe, T. S., Dziembowski, W. A., Judge, P. G., Snow, M., 2007, ApJ, 723, 213

Metcalfe, T. S., Basu, S., Henry, T. J., Soderblom, D. R., Judge, P. G., Knölker, M., Mathur, S., Rempel, M., 2010, ApJ, 723, 213

Moreno-Insertis, F. & Solanki, S. K. 2000, MNRAS, 313, 411

Otí Floranes H., Christensen-Dalsgaard J., Thompson M. J., 2005, MNRAS, 356, 671

Roxburgh I. W., Vorontsov S. V., 2003, A&A, 411, 215

Roxburgh I. W., 2005, A&A, 434, 665

Pallé, P. L., Régulo, C., Roca-Cortés, T., 1989, 224, 253

Pallé, P. L., Régulo, C., Roca-Cortés, T., 1990a, in: Progress of Seismology of the Sun and Stars, p. 129, eds. Osaki Y. & Shibahashi H., Springer-Verlag, Berlin

Pallé, P. L., Régulo, C., Roca-Cortés, T., 1990b, in: Progress of Seismology of the Sun and Stars, p. 189, eds. Osaki Y. & Shibahashi H., Springer-Verlag, Berlin

Rabello-Soares, M. C., Korzennik, S. G., Schou, J., 2008, AdSpR, 41, 861

Ritzwoller, M. H., Lavely, E. M., 1991, ApJ, 369, 557

Salabert, D., Fossat, E., Gelly, B., Kholikov, S., Grec, G., Lazrek, M., Schmider, F. X., 2004, A&A, 413, 1135

Salabert, D., García, R. A., Pallé, P., Jiménez-Reyes, S. J., 2009, A&A, 504, L1

Sheeley, N. J., 2010, in: Proc. SOHO-23: Understanding a Peculiar Solar Minimum, eds. S. Crammer, T. Hoeksema & J. Kohl, ASPCS, in the press (arXiv1005.3834v1)

Tapping K. F., DeTracey B., 1990, Sol Phys, 127, 321

Tripathy, S. C., Jain, K., Hill, F., Leibacher, J. W., 2010, ApJ, 711, L84

Toutain, T., Wehrli, C., 1997, in ASP Conf. Ser. 118: 1st Advances in Solar Physics Euroconference. Advances in Physics of Sunspots, ASP Conf. Ser. Vol. 118., Eds.: B. Schmieder, J.C. del Toro Iniesta, M. Vazquez, p. 254.

Verner, G. A., Chaplin, W. J., Elsworth, Y., 2006, MNRAS, 640, L95

Watson, F., Fletcher, L., Dalla, S., Marshall, S., 2009, SolPhys, 260, 5

Woodard, M. F., Noyes, R. W., 1985, Nat, 318, 449